

Design and Kinematic Modeling of Constant Curvature Continuum Robots: A Review

Robert J. Webster III¹ and Bryan A. Jones²

Abstract

Continuum robotics has rapidly become a rich and diverse area of research, with many designs and applications demonstrated. Despite this diversity in form and purpose, there exists remarkable similarity in the fundamental simplified kinematic models that have been applied to continuum robots. However, this can easily be obscured, especially to a newcomer to the field, by the different applications, coordinate frame choices, and analytical formalisms employed. In this paper we review several modeling approaches in a common frame and notational convention, illustrating that for piecewise constant curvature, they produce identical results. This discussion elucidates what has been articulated in different ways by a number of researchers in the past several years, namely that constant-curvature kinematics can be considered as consisting of two separate submappings: one that is general and applies to all continuum robots, and another that is robot-specific. These mappings are then developed both for the single-section and for the multi-section case. Similarly, we discuss the decomposition of differential kinematics (the robot's Jacobian) into robot-specific and robot-independent portions. The paper concludes with a perspective on several of the themes of current research that are shaping the future of continuum robotics.

Keywords

Manipulation, grasping, manipulation and compliant assembly, dynamics, *mechanics*, design and control, continuum robot, kinematics, hyperredundant robot, biologically inspired robot

1. Introduction

Biology has inspired researchers in many ways, and there are few fields of study where this is more clearly evident than in continuum robotics. The incredible capabilities for locomotion, manipulation, and dexterity in cluttered environments exhibited by snakes, elephant's trunks, tongues, and octopus tentacles have naturally inspired researchers to work toward recreating their capabilities in electromechanical devices. Recent progress toward this end has made modern continuum robotics a rapidly expanding area of research which promises to extend the use of robots into many new environments where they have not traditionally been applicable. A continuum robot can be defined as a continuously bending, infinite-degree-of-freedom robot with an elastic structure (see Figure 1 for some examples). Continuum robots are thus related to, but distinct from, hyperredundant robots which consist of (finitely) many short, rigid links (see Figure 1 for an example). Use of continuum robots in practical applications requires models of robot shape and motion. Such models must necessarily be more complex than those of traditional robots, which have a small number of rigid links. The

purpose of this paper is to provide an overview of the state of the art in continuum robot design and forward and differential kinematic modeling for both single-section and multi-section manipulators.

Our review is motivated by several factors. First, several years have elapsed since the most often-cited reviews of continuum robotics (Hirose 1993; Robinson and Davies 1999), during which many important advancements have been made. This has motivated two new review papers within the past year focusing on locomotion of mobile snake-like robots (Transeth et al. 2009) and the biological

¹ Department of Mechanical Engineering, Vanderbilt University, VU Station B 351592, Nashville, TN, USA

² Department of Electrical and Computing Engineering, James Worth Bagley College of Engineering, Mississippi State University, Mississippi State, MS, USA

Corresponding author:

Robert J Webster III, Department of Mechanical Engineering, Vanderbilt University, VU Station B 351592, 2301 Vanderbilt Place, Nashville, TN, 37235, USA
Email: robert.webster@vanderbilt.edu

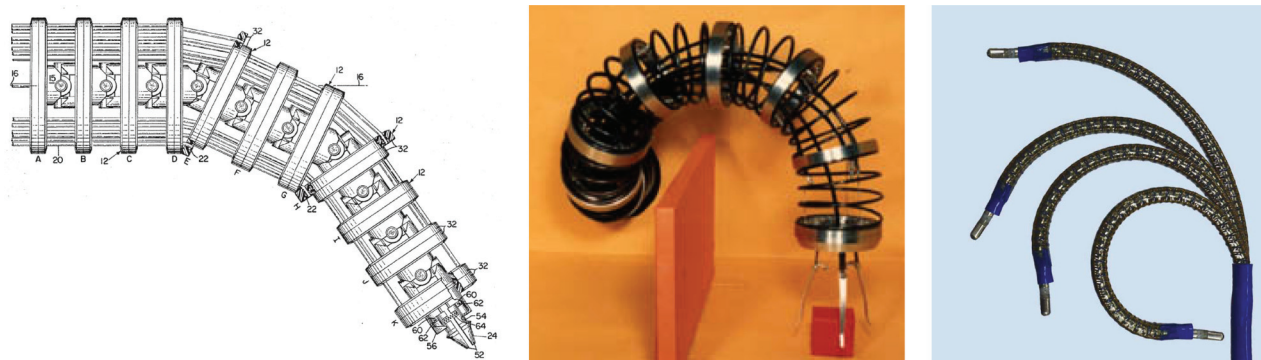


Fig. 1. (Left) The Tensor Arm of Anderson and Horn (1967) is generally regarded to be the first example of a hyperredundant robot. (Center) The subsequent work of Hirose (1993) was the first sustained research program in continuum and hyperredundant robots, beginning in the 1970s (image courtesy of Shigeo Hirose, and used by permission of Oxford University Press). (Right) An example of a modern continuum robot used for medical applications is the Hansen Medical Sensei[®] system, the kinematics and mechanics of which have been described by Camarillo et al. (2008) (image courtesy of David Camarillo, © 2008 IEEE).

inspiration and design of soft (particularly pneumatic) continuum robots (Trivedi et al. 2008b). These are complementary to our current review of constant-curvature kinematics, with little overlap. Second, the diversity of applications (see Section 2) for continuum robots leads to a widely distributed literature, which can make it challenging for newcomers to the field to collect all relevant results expeditiously. An additional layer of complexity in interpreting results is the variety of mathematical formalisms and coordinate frame choices employed. Similarly, the distinction between robot-specific and robot-independent results can be subtle, which has led to some of the same results being re-demonstrated in a number of papers, including the authors' own work. Interestingly and productively, if it is clear that multiple approaches can achieve the same results, this re-demonstration provides a variety of techniques for continuum robot kinematics, each of which may have unique advantages for future modeling, design, and real-time implementation efforts. Furthermore, the results in this paper will be particularly useful for a newcomer to the field of continuum robotics who desires simple and straightforward answers to questions such as "What is known about continuum robots?" and "How can I describe the shape and motion of my new continuum robot design?"

Unlike kinematics for traditional rigid-link robots where the pose of any point on the robot can be fully defined (in closed form) by link lengths and joint angles, the inherent compliance of continuum robots requires consideration of elasticity. To accurately define the pose of points of interest on the robot (including its end-effector), one must characterize forces and moments applied to the robot by both its own actuators and the external environment. The most general models available for this (see, e.g., Ivanescu et al. (2007), Gravagne et al. (2003), Trivedi et al. (2008a), Rucker et al. (2010a), Rucker et al. (2010b), Dupont et al. (2010), Chirikjian (1995), and Jones et al. (2009)) do not do so in closed form. Instead, they are evaluated numerically to compute statics or dynamics in lieu of

forward kinematics. Although some preliminary work exists in the real-time evaluation of these models (Jones et al. 2009), it is not yet clear whether such results can be used to develop real-time Jacobians or can otherwise be applied to facilitate closed-loop control of continuum robots in a wide variety of applications.

Thus, both before and after the development of these general models, researchers have sought suitable simplifying assumptions and approximations that can be accurate enough for practical implementation and are more analytically tractable. One approach begins by describing the space curves desired, then fitting the physical robot (as nearly as possible) to these theoretical curves (see, e.g., Andersson (2008)). For example, clothoid curves have been proposed based on careful observations of biological snakes and are particularly useful for mimicking biological snake locomotion (Hirose 1993; Hirose and Yamada 2009). Extending the basic approach of fitting the physical manipulator to analytically desirable mathematical curves, the work of Chirikjian and Burdick (1994) defines a curve as the product of a Bessel function with sines and cosines which enables a modal approach to inverse kinematics. Similarly, wavelets are applied by Gravagne (2002) to describe the shape of a continuum robot.

An alternative simplifying approach that permits closed-form kinematics and facilitates closed-form Jacobian formulation is to approximate the robot as a series of mutually tangent constant-curvature arcs ("piecewise constant curvature"). While most continuum robots are composed of arcs that are not perfectly circular, many are approximately so (see, e.g., Xu and Simaan (2008), Neppalli and Jones (2007), and Webster et al. (2009)). The remarkable usefulness of the piecewise constant-curvature approximation across a wide variety of continuum robot mechanical architectures (discussed in Section 2) combined with its analytical attractiveness has led to broad application of this modeling approach. Thus, we focus on piecewise constant-curvature kinematics in this paper, before

returning in Section 6 to consider the future prospects for both constant and variable curvature modeling and design.

1.1. Contribution

In this paper we contribute a unification of recent kinematic and differential kinematic results for both single-section and multi-section piecewise constant-curvature continuum robotics into a common coordinate frame and notational convention, filling in small gaps in the literature where they exist. We demonstrate that several different modeling approaches produce a single, common result for piecewise constant-curvature forward kinematics and we clearly delineate the boundaries of robot-specific and robot-independent mappings for both forward and differential kinematics. We also provide a brief historical perspective on continuum robots, discuss some of the basic mechanical designs that have been developed, and provide a perspective on the themes that are shaping future research in continuum robotics.

2. Origin, Design, and Applications of Continuum Robots

The origin of continuum robotics is generally traced back to the creation of serpentine robots in the late 1960s (see Moran (2007, p. 110) and Rosheim (1994, pp. 110–121)). These hyperredundant robots employed a number of closely spaced joints to emulate the motion of the backbone of a snake. Examples include the Orm, which consisted of a series of pneumatically controlled bellows (see Nocks (2007, p. 68) and Thring (1983)), and the tensor arm (Anderson and Horn 1967, 1970), a tendon-driven robot intended for underseas applications. The weaknesses of the continuum design at that time, which included low payload, poorly understood kinematics and dynamics, and coarse positioning accuracy, prompted the abandonment in the 1970s of promising research projects that began in the late 1960s (Moran 2007).

Sustained development of continuum and hyperredundant robots re-emerged in the late 1970s and continued throughout the 1980s and beyond with the pioneering work of Hirose and his team, who developed many novel and innovative designs, paying particular attention to inspiration gleaned from biological systems. Much of this work is summarized in Hirose (1993). Industrial continuum manipulators developed during this time period include the Spine robot, a high-dexterity spray-painting robot (Larson and Davidson 1985), while other academic efforts included the creation of trunk-like manipulators (Wilson et al. 1993; Morecki et al. 1987), and miniature pneumatic or hydraulic actuators applied as robot fingers (Suzumori et al. 1992). Significant progress in modeling continuum robots was made in the 1990s, including the introduction of a modal approach (Chirikjian and Burdick 1994; Chirikjian 1995; Chirikjian and Burdick 1995) establishing a theoretical foundation for continuum robotics based on approximating

the shape of a continuum robot using a mathematically tractable curve. Other significant contributions included modeling the underlying continuum mechanics of the robot (Ivanescu and Stoian 1995). In addition, continuum robots continued to be applied in many new and innovative applications in both the commercial (Immega and Antonelli 1995) and academic research (Robinson and Davies 1999) forums.

The first decade of the 21st century has seen a great deal of advancement in the design, modeling, and application of continuum robotics. Much foundational work establishing the theoretical framework for analysis of continuum robots early in this decade has come from the group of Walker et al. (Gravagne et al. 2003; Gravagne and Walker 2002; Hannan and Walker 2003; Jones and Walker 2007, 2006a,b; Neppalli et al. 2009). Active areas of current research by many groups include continued advancement in the application of beam theory to create increasingly sophisticated models of continuum robots (see, e.g., Gravagne et al. (2003), Camarillo et al. (2008), Webster et al. (2009), Rucker et al. (2010a), Dupont et al. (2010), and Trivedi et al. (2008a)), and the elucidation of various parsimonious modeling simplifications, including the constant-curvature approximation (see, e.g., Hannan and Walker (2003), Jones and Walker (2006a), and Webster et al. (2009)).

Many practical applications for continuum and hyperredundant robots have been suggested and/or demonstrated (as shown in Table 1), including undersea manipulation (Anderson and Horn 1967; Lane et al. 1999), car painting (Hirose 1993; Larson and Davidson 1985), nuclear decontamination (Immega and Antonelli 1995), nuclear reactor repair (OC Robotics 2008), waste storage tank remediation (see <http://www.templeallen.com/>), liquid transport (Ciésłak and Morecki 1999), sanding (see <http://www.templeallen.com/>), inspection of unstructured environments and pipes (Wakahara et al. 1984; Paljug et al. 1995; Osuka and Kitajima 2003; Suzumori et al. 2003; Takahashi et al. 1994; Wolf et al. 2003), and search and rescue (Tsukagoshi et al. 2001; Aoki et al. 2002).

Continuum robots have also made a significant impact in medicine. A large number of commonly used medical devices such as catheters and colonoscopes can be considered continuum devices. While commonly applied as manually operated instruments, noteworthy efforts have been made to robotize these and other continuum devices for surgery including forceps (Nakamura et al. 1995), flexible needles (Webster et al. 2006a), laparoscopic tools (Peirs et al. 2003), endoscopes (Ikuta et al. 1988), arthroscopes (Dario et al. 2000), colonoscopes (Phee et al. 1997), laser manipulators (Harada et al. 2007), and catheters (Ohta 2001; Camarillo et al. 2008), among others. Examples of continuum robots developed specifically for surgical applications that do not directly mimic existing surgical devices include the multibackbone throat surgery system of Xu and Simaan (2008), the hyperredundant Cardio Arm of Degani et al. (2006), and the concentric-tube active

Table 1. A sampling of snake-like robot designs the shape of which has been or could be described using constant-curvature kinematics. Intended to be exemplary, not comprehensive. Inspired by the classifications of Simaan et al. (2004), Hirose (1993), and Robinson and Davies (1999).

Literature	Classification criteria								
	Continuous/ discrete	Extensible	Number of sections	Actuators/ section	DOF/ section	Actuator spacing	Actuation	Multi-section coupling**	Application
Tensor arm (Anderson and Horn 1967, 1970)	D		4	4	2	90°	Tendon	Co-radial	Underwater manipulation
OCRobotics (Buckingham 2002; Robotics 2008)	D		5	3	2	120°	Tendon	Distributed	Reactor repair
Elephant trunk (Hannan and Walker 2003)	D		4	4	2	90°	Tendon/spring	Co-radial	Bioinspired manipulation
Elephant trunk (Ciésłak and Morecki 1999)	C		3	2	2	90°	Tendon/spring	Co-radial	Liquid transportation
EMMA (Bostelman et al. 1997) (see also http://www.templeallen.com/)	D		3	3	2	120°	Tendon/spring	Co-radial	Sanding, nuclear
Backbone (Gravagne et al. 2003)	C		1	1	1	180°	Tendon/rod	N/A	General purpose
Tentacle robot (Li and Rahn 2002)	C		2	4	2	90°	Tendon/rod	Co-radial	General purpose
Arthroscope (Dario et al. 2000)	D		1	1	2	180°	Tendon/rods	N/A	Arthroscopy
Catheter (Camarillo et al. 2008, 2009a)	C	◦	2	2	3	90°	Tendon/sleeve	Distributed	Cardiac surgery
Colobot (Chen et al. 2004, 2005, 2006)	C	◦	1	3	3	120°	Pneumatic	N/A	Colonoscopy
OctArm (Jones and Walker 2006a,b)	C	◦	3	3	3	120°	Pneumatic	Individual	General purpose
Slim Slime 1 (Ohno and Hirose 2000, 2001)	C	◦	6	3	3	120°	Pneumatic	Individual	Search and rescue
Slim Slime 2 (Aoki et al. 2002, 2004)	C	◦	2	3	3	120°	Tendon/pneumatic	Co-radial	Search and rescue
Air-OCTOR (Jones and Walker 2006b)	C	◦	2	3	3	120°	Tendon/pneumatic	Distributed	General purpose
KSI (Immega 1994; Immega and Antonelli 1995; Immega et al. 1995)	C	◦	2	3	2	120°	Tendon/pneumatic	Distributed	Nuclear decontamination
Active catheter (Bailly and Amirat 2005)	C	◦	3	3	2	120°	Hydraulic	Individual	Cardiac surgery
DDU (Simaan et al. 2004; Xu and Simaan 2008)	C		3	3	2	120°	Multibackbone	Co-located	Laryngeal surgery
Active cannula (Dupont, et al. 2010; Webster et al. 2009)	C	◦	2 <i>n</i>	1	2	–	<i>n</i> curved tubes	*	Surgical dexterity
Beveled needle (Webster et al. 2006a)	C	◦	∞	0	3	–	Tip/tissue	Individual	Surgical dexterity

*Could be considered co-located or continuously distributed: see Section 3.2.3.

**See Section 4.

cannula of Webster et al. (Webster et al. 2006b; Rucker and Webster 2009b; Webster et al. 2009; Rucker et al. 2010a, b), also developed independently and concurrently by Dupont et al. (Sears and Dupont 2006, 2007; Dupont et al. 2009, 2010), which is described in Section 3.2.3. In Table 1, “Surgical dexterity” refers to the ability to curve or steer what have traditionally been straight devices such as needles or rigid laparoscopic shafts, enabling them to “turn corners” inside the human body.

Earlier classifications of continuum robots have based their taxonomy on the location of mechanical actuation (Robinson and Davies 1999), on the backbone architecture, extensibility, and actuation (Simaan et al. 2004), or presented a series of continuum robot prototypes (Hirose 1993). A review of soft robotics (Trivedi et al. 2008b) contrasts rigid, hyperredundant, hard continuum, and soft robots and provides a broader overview of biologically inspired robotics including robotic fish, starfish, trunks, worms, and other creative realizations of soft robots. All of the above are useful ways to categorize continuum and hyperredundant robots, and we draw inspiration from them in compiling Table 1. However, our purpose here is not a comprehensive taxonomy (given the rapidly accelerating recent interest in continuum and hyperredundant robots, such an objective would be perhaps prohibitively challenging), but rather we seek to illustrate the diversity of designs for which the constant-curvature forward and differential kinematics we describe in the remainder of this paper are applicable. Here, we omit the subset of hyperredundant robots where constant curvature has not been a primary consideration, either because the robot commonly takes on other shapes, or because the links are long enough that constant curvature is not a useful approximation. This is in no way intended to diminish this very useful class of robot (examples include Hirose and Ma (1991), Paljug et al. (1995), Chirikjian and Burdick (1994), Ebeert-Uphoff and Chirikjian (1996), Suthakorn and Chirikjian (2001), and Wright et al. (2007)), and reviews of many of these, particularly those that locomote in a snake-like manner, are available to the interested reader in Hirose (1993) and Transteth et al. (2009).

Table 1 illustrates the mechanical diversity of continuum robots that approximate piecewise constant curvature. Backbones may be continuous or discrete (hyperredundant robots), and some designs include extensible backbones. Continuum robots consist of multiple serially linked sections. Each section bends with between one degree of freedom (DOF) (e.g. an inextensible planar robot) and three DOFs (i.e. an extensible robot that can bend about two axes without axial rotation). Continuum robots may be under- or over-actuated, meaning that they can have fewer or more actuators than DOFs. An example of a prevalent over-actuated design is one whose cables lie at 90° intervals about the central axis (see, e.g., Hannan and Walker (2003)). An example of an under-actuated robot is a cardiac catheter that uses four wires to actuate two 3-DOF sections (Camarillo et al. 2009a). Many different actuation

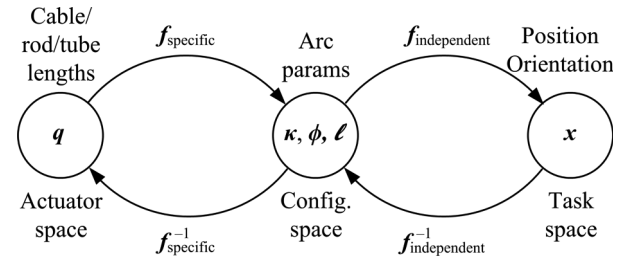


Fig. 2. The three spaces and mappings between them which define the kinematics of constant-curvature robots. A robot-specific mapping, discussed in Section 3.2, transforms actuator space variables q to configuration space variables (κ, ϕ, ℓ) . Next, a robot-independent mapping takes these configuration space variables to the task space, as developed in the following section. Section 4.2 reviews inverse mappings for both the robot-specific and the robot-independent cases.

strategies can and have been used, and a few robots are designed to bend only in one plane, to enable enhanced payload capability (see, e.g., Hirose and Ma (1991)) or for simplicity of model verification (e.g. the experimental setup in Li and Rahn (2002)). There have also been a number of approaches to coupling multiple sections together (see the second column from the right in Table 1). In the table, single-section robots are marked N/A, multi-section robots in which each section is mechanically uncoupled from other sections, such as that of Jones and Walker (2006a), are labeled “Individual”, and some other options for actuator routing are illustrated in Figure 14, and discussed further in Section 4.

We proceed in subsequent sections of this paper to address the kinematic modeling of robots such as those in Table 1 that may be approximated as piecewise constant curvature. Section 3 describes constant-curvature kinematics, Section 4 addresses multi-section forward and inverse kinematics, and Section 5 describes constant-curvature differential kinematics.

3. Piecewise Constant Curvature Kinematics

Constant curvature has often been viewed as a desirable characteristic in continuum robots due to the simplifications it enables in kinematic modeling. Variable curvature elastic structures (Kim and Chirikjian (2006)) are described by functions that are integrated, whereas constant-curvature robots can be considered as consisting of a finite number of curved links. These links are described by a finite set of arc parameters, which can be converted into analytical frame transformations, as discussed in this section. Thus, constant curvature can facilitate additional analysis on topics such as differential kinematics, real-time control, etc.

The constant-curvature approximation has been successfully applied to many continuum robots. For example, if a constant moment is applied along a beam, Bernoulli–Euler beam mechanics predict a constant-curvature result (Gragvagne et al. 2003). This is the case for the initial simple

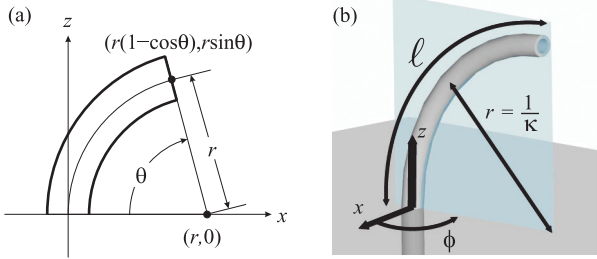


Fig. 3. (a) When ϕ is zero, the arc lies in the x - z plane as shown. (b) The angle ϕ rotates the arc out of the x - z plane. The “arc parameters” that describe a circular arc, namely curvature (κ), plane (ϕ), and arc length (ℓ), are shown. The axes shown in both figures are those of the fixed spatial frame.

models derived for the active cannula design described in Section 3.2.3, in which concentric precurved tubes (under the torsionless assumption) directly apply constant moments to one another. Arguments of Li and Rahn (2002) demonstrate that a constant moment can be applied by a cable terminating at the end of a flexible rod and passing through a sufficient number of cable guides fixed along the rod (see Section 3.2.2). Likewise, the pneumatically actuated trunks described in Section 3.2.1 can be considered piecewise constant curvature because the actuators closely approximate the application of a moment to the end of the trunk (Jones and Walker 2006a). Many other continuum robots have also been observed to exhibit approximate constant curvature (e.g. Hannan and Walker (2003), Simaan et al. (2004), Anderson and Horn (1967), Hirose (1993), Ciésłak and Morecki (1999), and Immega and Antonelli (1995), among others).

The piecewise constant-curvature assumption has the advantage of enabling kinematics to be decomposed into two mappings (Jones and Walker 2006a), as visualized in Figure 2. One is from joint or actuator space, \mathbf{q} , to configuration space parameters that describe constant-curvature arcs. The other is from this configuration space to task space, consisting of a space curve which describes position and orientation along the backbone. Examples of actuator variables include lengths of cables, flexible push rods, or pneumatic tubes. Arc parameters, which define the configuration space of the robot, consist of triplets of curvature ($\kappa(\mathbf{q})$), the angle of the plane containing the arc ($\phi(\mathbf{q})$), and arc length ($\ell(\mathbf{q})$, or sometimes $s \in [0, \ell]$), as shown in Figure 3(b). Alternatively, the relationship $\theta = \kappa s$ allows parameterization based on the angle θ through which the arc bends (see, e.g., Simaan et al. (2009)).

The mapping $\mathbf{f}_{\text{specific}}$ from actuator space \mathbf{q} to the configuration space of arc parameters (κ, ϕ, ℓ) is robot-specific, since actuators in each unique robot design influence arc parameters in different ways. In particular, consideration of the forces and moments applied by actuators coupled with suitable approximations (e.g. the application of a constant moment as discussed earlier) yields this mapping from actuator variables (pressure, length, etc.) to circular sections described by arc parameters in configuration

space. In contrast, the mapping $\mathbf{f}_{\text{independent}}$ from arc parameters to pose \mathbf{x} along the backbone is robot-independent because it is applicable to all systems that can be approximated as piecewise constant-curvature arcs. This is a purely kinematic mapping, transforming from arc parameters to a space curve in task space. In the following sections, we first describe methods of accomplishing the robot-independent mapping, then proceed to consider several case studies on the robot-specific mapping for robots with varying types of actuators.

3.1. The Robot-independent Mapping

A wide variety of conventions, formalisms, and coordinate frame choices exist in the literature to accomplish forward kinematics. In this section, we show that the various methods all fundamentally produce the same result for piecewise constant-curvature robots. To illustrate this, we choose a frame convention and use it throughout the paper, recasting results from the literature using this convention, which Figure 3 illustrates. Specifically, we consider the $+z$ -axis to be tangent to the base of the continuum robot. When $\phi = 0$, positive curvature ($\kappa > 0$) produces bending about the $+y$ -axis such that when the continuum robot backbone has traced out an angle of π radians it will touch the $+x$ -axis. In the following, we describe several different approaches to derive the position and orientation of the centerline of the robot.

Referring to Figure 2, this section therefore defines $\mathbf{f}_{\text{independent}}$ in terms of the homogeneous transformation matrix T parameterized by (κ, ϕ, ℓ) . This matrix gives task space coordinates $\mathbf{x} = T_{1...3,4}$. This section begins development of this mapping with a geometric argument.

3.1.1. Arc Geometry. The geometry of a continuum robot provides a means of determining the pose of points along it (Hannan and Walker 2003; Bailly and Amirat 2005; Neppalli and Jones 2007; Webster 2007). In Figure 3(a), when $\phi = 0$ the coordinates of a point on the circular arc of radius r in the x - z plane centered at $[r \ 0 \ 0]^T$ are $\mathbf{p} = [r(1 - \cos \theta) \ 0 \ r \sin \theta]^T$. Note also that this motion includes a rotation $R_y(\theta)$ about the $+y$ -axis, where $R_y(\theta) \in \text{SO}(3)$ indicates a rotation about the y -axis by the angle θ . Rotating the entire arc about the $+z$ -axis by ϕ moves the robot out of the x - z plane, producing a transformation from arc base to tip,

$$T = \underbrace{\begin{bmatrix} R_z(\phi) & 0 \\ 0 & 1 \end{bmatrix}}_{\text{Rotation}} \underbrace{\begin{bmatrix} R_y(\theta) & \mathbf{p} \\ 0 & 1 \end{bmatrix}}_{\text{Inplane transformation}}. \quad (1)$$

Noting that $\kappa = 1/r$ and $\theta = \kappa s$ (where $s \in [0, \ell]$), this can be written in terms of arc parameters (κ, ϕ, ℓ) as follows. Here, to emphasize that this transformation can be written at any point s along the arc from 0 to ℓ we use the symbol s and write,

Table 2. D-H parameter table for a single section of a piecewise constant-curvature continuum robot, as given in Figure 4. Here “link” refers to the several imaginary robot links used to model a single section of a continuum robot. Mappings from D-H to arc parameters derived in the text are included.

Link	ϑ	d	a	α
1	$\vartheta_1 = \phi$	0	0	$-\pi/2$
2	$\vartheta_2 = \kappa s/2$	0	0	$\pi/2$
3	0	$d_3 = (2/\kappa)\sin \kappa s/2$	0	$-\pi/2$
4	$\vartheta_4 = \kappa s/2$	0	0	$\pi/2$
5	$\vartheta_5 = -\phi$	0	0	0

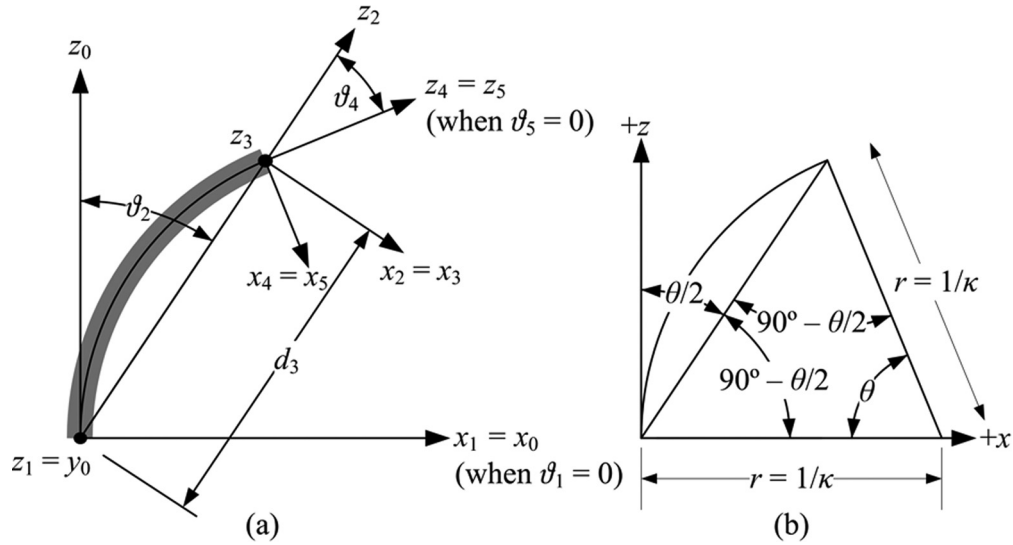


Fig. 4. (a) D-H axes used to construct a hypothetical rigid-link representation of a continuum robot with the same tip frame as the actual continuum robot. The resulting D-H table is given in Table 2. All vectors remain in the plane, except for z_1 and z_3 which extend out of the paper and are therefore diagrammed as dots. (b) Given an arc which cuts through θ degrees extending from the origin tangent to the $+z$ -axis and bending about the $+y$ -axis, per the conventions established in this paper, the angle between the z -axis and a line connecting the origin to the arc tip is $\theta/2$.

$$T_w = \begin{bmatrix} \cos^2 \phi (\cos \kappa s - 1) + 1 & \sin \phi \cos \phi (\cos \kappa s - 1) & \cos \phi \sin \kappa s & \frac{\cos \phi (1 - \cos \kappa s)}{\kappa} \\ \sin \phi \cos \phi (\cos \kappa s - 1) & \cos^2 \phi (1 - \cos \kappa s) + \cos \kappa s & \sin \phi \sin \kappa s & \frac{\sin \phi (1 - \cos \kappa s)}{\kappa} \\ -\cos \phi \sin \kappa s & -\sin \phi \sin \kappa s & \cos \kappa s & \frac{\sin \kappa s}{\kappa} \\ 0 & 0 & 0 & 1 \end{bmatrix}. \quad (3)$$

$f_{\text{independent}} =$

$$T = \begin{bmatrix} \cos \phi \cos \kappa s & -\sin \phi & \cos \phi \sin \kappa s & \frac{\cos \phi (1 - \cos \kappa s)}{\kappa} \\ \sin \phi \cos \kappa s & \cos \phi & \sin \phi \sin \kappa s & \frac{\sin \phi (1 - \cos \kappa s)}{\kappa} \\ -\sin \kappa s & 0 & \cos \kappa s & \frac{\sin \kappa s}{\kappa} \\ 0 & 0 & 0 & 1 \end{bmatrix}. \quad (2)$$

Note that the tip frame in (1) and (2) is aligned so that the x -axis points toward the center of the circle. In some applications (e.g. when a gripper is attached to the tip of the arc), it may be useful to orient the tip frame such that it aligns

with the base frame when “slid” along the arc to the base without rotation about the local z -axis (that is, use of a Bishop’s frame (Bishop 1975)). This can be obtained by post-multiplying T by a homogeneous transformation with rotation $R_z(-\phi)$ and translation $\mathbf{0}$, yielding an alternate $f_{\text{independent}}$ given in (3) on the following page.

As we review in the remainder of this section, these results can and have been derived in a variety of ways, including via Denavit–Hartenburg (D-H) parameters (Hannan and Walker 2003), Frenet–Serret (F-S) frames (Hannan and Walker 2003), a similar integral formulation that can account for zero curvature (Chirikjian and Burdick 1994) (the F-S frame is undefined when curvature equals zero), and exponential coordinates (Sears and Dupont 2006;

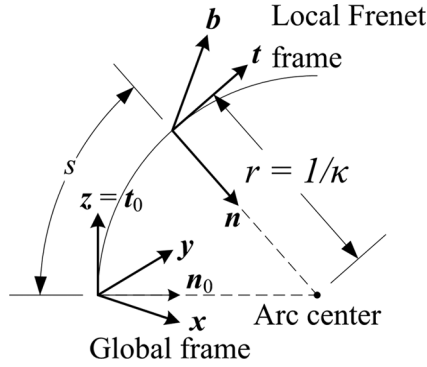


Fig. 5. An illustration of the Frenet–Serret coordinate frame used to describe a constant-curvature continuum robot. This local coordinate frame consists of a vector \mathbf{t} tangent to the curve, a vector \mathbf{n} normal to the curve, and a binormal vector \mathbf{b} to complete the frame. The constant curvature κ defines the radius of the resulting arc, while the initial condition \mathbf{n}_0 defines the angle of the plane containing the arc. The choice of \mathbf{t}_0 to lie along the $+z$ -axis causes the curve to extend along that axis, per convention.

Webster et al. 2006a, 2009). Our review highlights the fact that while derivations in the literature may appear different at first glance due to the diversity of frame choices, formalisms, and symbols employed, they arrive at the same final result when piecewise constant curvature is assumed.

3.1.2. D-H Parameters. Forward kinematics for a segment of a piecewise constant-curvature robot as given in (2) and (3) can be derived using the D-H method, augmented with transformations between D-H parameters and arc parameters (ϕ, κ, ℓ) . In this section, ϑ_i variables describe rotations about the local z -axis, not to be confused with the separate use of θ to define the angle through which the arc bends as shown in Figure 3(a). One D-H table and mapping, given in Jones and Walker (2006a), models a single curved arc as consisting of a first pair and final pair of ball-and-socket joints. Another approach introduced in Hannan and Walker (2003) decomposes the problem, in a manner similar to the geometric argument above, as an inplane transformation together with a rotation of the arc about the z -axis by $\vartheta_1 = \phi$.

Following this second approach, the inplane transformation (whose D-H parameters are given in links 2–4 of Table 2) is illustrated in Figure 4(a). This is constructed by first rotating about z_1 by ϑ_2 to point z_2 toward the continuum robot’s tip, then translating by d_3 along z_2 to move to the robot’s tip, and finally rotating about z_3 by ϑ_4 to align z_4 with the backbone tangent direction. As discussed in the previous section, an optional final rotation of ϑ_5 about z_4 provides an alternate choice of end-effector frame orientation. Note that the entries in Table 2 have been modified from Hannan and Walker (2003) so that the arc curves about the y -axis, following the convention established earlier.

The relationships between D-H parameters and arc parameters are given in Table 2. Insight on these relationships

can be obtained by observing that Figure 4 shows $\vartheta_2 = \vartheta_4 = \theta/2$ and $\vartheta_1 = \phi$. Tip coordinates in two dimensions, given in Figure 3(a), yield $d_3 = r \sqrt{2(1 - \cos \theta)} = 2r \sin \theta/2$ (since $1 - \cos \theta = 2 \sin^2 \theta/2$). The relationships $\theta = \kappa s$ and $\kappa = 1/r$ complete the mapping. With these relationships, the D-H table corresponds to the transformation given in (2). Including the optional ϑ_5 yields (3).

3.1.3. Frenet–Serret Frames. Differential calculus provides a rich set of tools for describing the evolution of a curve in space, forming the basis for describing the static and dynamic behavior of non-linearly elastic rods (Antman 2005). In particular, use of the F-S formulas provide a third means of deriving the forward kinematics of piecewise constant curvature robots. Reviewing Hannan and Walker (2003), the F-S equations parameterize a curve in terms of arc length s by defining a local coordinate frame shown in Figure 5 which moves along the curve in terms of a unit vector tangent to the curve $\mathbf{t}(s)$, a unit vector $\mathbf{n}(s)$ which is normal to the curve, and a unit binormal vector $\mathbf{b}(s) = \mathbf{t}(s) \times \mathbf{n}(s)$ perpendicular to both the tangent and normal vectors. Two functions, the curvature $\kappa(s)$ and torsion $\tau(s)$, determine the evolution of the curve as

$$\begin{aligned} \mathbf{t}'(s) &= \kappa(s)\mathbf{n}(s), \\ \mathbf{n}'(s) &= -\kappa(s)\mathbf{t}(s) + \tau(s)\mathbf{b}(s), \text{ and} \\ \mathbf{b}'(s) &= -\tau(s)\mathbf{n}(s), \end{aligned}$$

where the prime indicates differentiation with respect to s . Noting that many continuum robots are constructed to reduce torsion where possible, and recalling the constant-curvature assumption, $\kappa(s) \equiv \kappa$ and $\tau(s) \equiv 0$. The defining equations of a continuum robot are therefore $\mathbf{t}'(s) - \kappa\mathbf{n}(s) = 0$ and $\mathbf{n}'(s) = -\kappa\mathbf{t}(s)$. Differentiating and substituting, $\mathbf{t}''(s) + \kappa^2\mathbf{t}(s) = 0$. Solving,

$$\mathbf{t}(s) = \mathbf{t}_0 \cos \kappa s + \mathbf{n}_0 \sin \kappa s, \quad (4)$$

where $\mathbf{t}_0 = \mathbf{t}(0)$ and $\mathbf{n}_0 = \mathbf{n}(0)$.

To obtain coordinates along the curve $\mathbf{p}(\ell)$, it is possible to integrate the tangent vector

$$\mathbf{p}(\ell) = \int_0^\ell \mathbf{t}(s) ds = \mathbf{t}_0 \kappa^{-1} \sin \kappa \ell + \mathbf{n}_0 \kappa^{-1} (1 - \cos \kappa \ell). \quad (5)$$

Derivation of the above result for the planar case can be found in Hannan and Walker (2003), and it can be extended to three dimensions as follows. According to the convention established in the previous section, the $+z$ -axis is tangent to the continuum robot at its base, making the initial tangent vector $\mathbf{t}_0 = [0 \ 0 \ 1]^T$. The initial normal vector is perpendicular to \mathbf{t}_0 and depends on the direction of curvature defined by the angle ϕ , so that $\mathbf{n}_0 = [\cos \phi \ \sin \phi \ 0]^T$. Substituting these initial conditions into (4),

$$\mathbf{t}(s) = [\cos \phi \sin \kappa s \ \sin \phi \sin \kappa s \ \cos \kappa s]^T. \quad (6)$$

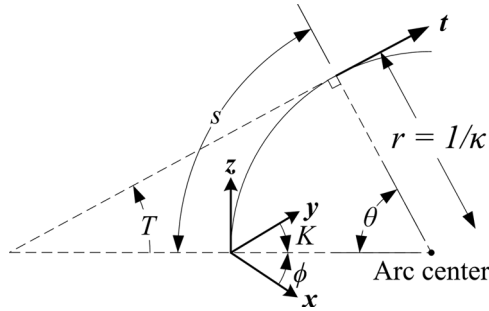


Fig. 6. The integral representation defines the tangent vector \mathbf{t} (given in (7)) to the arc in terms of one function ($K(s)$) which gives the angle in the x - y plane measured clockwise from the $+y$ -axis, and another ($T(s)$) which specifies the elevation. The connection to the arc parameters (κ, ϕ, ℓ) used throughout this paper can be made by observing that based on the geometry above $K = \pi/2 - \phi$ and $T = \pi/2 - \theta$, where $\theta = \kappa s$.

Integrating \mathbf{p} in (5) under these initial conditions produces a tip position identical to \mathbf{p} in (2).

The local coordinate frame vectors \mathbf{t} , \mathbf{n} , and \mathbf{b} provide orientation for the tip frame. First, note that the choice of an initial tangent vector \mathbf{t}_0 maps \mathbf{t} in the base frame to the $+z$ -axis. Likewise, the initial normal vector \mathbf{n}_0 points toward the center of the arc, agreeing with the frame convention established in Section 3.1.1, implying that the orientation is $R = [\mathbf{n} \ \mathbf{b} \ \mathbf{t}]$. Substituting (6) into the relationship $\mathbf{n}'(s) = -\kappa \mathbf{t}(s)$, we have

$$\mathbf{n}(s) = -\kappa \int [\cos \phi \sin \kappa s \quad \sin \phi \sin \kappa s \quad \cos \kappa s]^T ds$$

yielding $\mathbf{n}(s) = [\cos \phi \cos \kappa s \quad \sin \phi \cos \kappa s \quad -\sin \kappa s]^T$ and $\mathbf{b}(s) = \mathbf{t}(s) \times \mathbf{n}(s) = [-\sin \phi \quad \cos \phi \quad 0]^T$. Assembling these columns gives the rotational portion of the matrix in (2).

3.1.4. Integral Representation. While differential curve representations other than F-S are possible (see, e.g., Bishop (1975)), another approach given in Chirikjian and Burdick (1994) is the integral representation of a curve, also used in the dynamics formulation of Ivanescu et al. (2007). This integral formulation avoids difficulties which arise in the F-S formulas when $\kappa = 0$ and avoids the necessity of solving a differential equation to extract the curve, given arc length parameterized curvature and torsion functions.

Like the F-S approach, integration of a vector $\mathbf{t}(s)$ tangent to the curve at s determines the shape of the curve, where

$$\mathbf{t}(s) = \begin{bmatrix} l(s) \sin K(s) \cos T(s) \\ l(s) \cos K(s) \cos T(s) \\ l(s) \sin T(s) \end{bmatrix}. \quad (7)$$

In this equation, $l(s)$ specifies dilation, where $l = 1$ produces a curve that is neither compressed (when $l < 1$) or extended ($l > 1$). The angle $K(s)$ gives the orientation of

the tangent vector \mathbf{t} in the x - y plane, measured clockwise from the y -axis, and $T(s)$ gives the angle between \mathbf{t} and the x - y plane, as shown in Figure 6. From Chirikjian and Burdick (1994), tip position is defined as

$$\mathbf{p}(\ell) = \int_0^\ell \mathbf{t}(s) ds. \quad (8)$$

Applying this formulation to the constant-curvature inextensible case implies that $l(s) \equiv 1$. Referring again to Figure 6 or, equivalently, setting (7) equal to (6), the angles

$$\begin{aligned} K(s) &= \pi/2 - \phi \\ T(s) &= \pi/2 - \kappa s \end{aligned} \quad (9)$$

define a vector \mathbf{t} tangent to a constant-curvature arc using the frame convention chosen for this paper. With these definitions, integrating (8) produces a tip position identical to \mathbf{p} in (2) and (3).

With respect to orientation, Chirikjian and Burdick (1994) defined an “induced” reference frame along the backbone, which differs from the F-S frame by a rotation about the tangent vector. To see how this representation agrees with (2) for the constant-curvature case, one must simply relabel axes (Chirikjian and Burdick (1994) has the \mathbf{e}_2 or y -axis of the local frame tangent to the curve) such that the frame remains right handed, with \mathbf{e}_3 (or z) tangent to the curve. This results in a shuffling of the columns of the induced rotation matrix Q_{IR} provided in Chirikjian and Burdick (1994). Then, substituting (9) into the resulting Q_{IR} yields the rotation matrix given in (2).

3.1.5. Exponential Coordinates. Similar results can be obtained using exponential coordinates based on Lie group theory (Sears and Dupont 2006; Webster et al. 2006a, 2009). See also Murray et al. (1994) for a thorough treatment of exponential coordinates – in this section we follow the notation and conventions outlined therein. Recalling from (1) that the homogeneous transformation for a circular arc can be decomposed into a rotation and an inplane transformation, we can write the twist coordinates associated with each as

$$\mathbf{x}_{\text{rot}} = \begin{bmatrix} \mathbf{v}_{\text{rot}} \\ w_{\text{rot}} \end{bmatrix} = [0 \ 0 \ 0 \ 0 \ 0 \ 1]^T \quad \text{and} \quad (10)$$

$$\mathbf{x}_{\text{inp}} = \begin{bmatrix} \mathbf{v}_{\text{inp}} \\ w_{\text{inp}} \end{bmatrix} = [0 \ 0 \ 1 \ 0 \ \kappa \ 0]^T, \quad (11)$$

respectively, where \mathbf{v} and w are linear and angular differential motions. Then, writing the twist coordinates as twists,

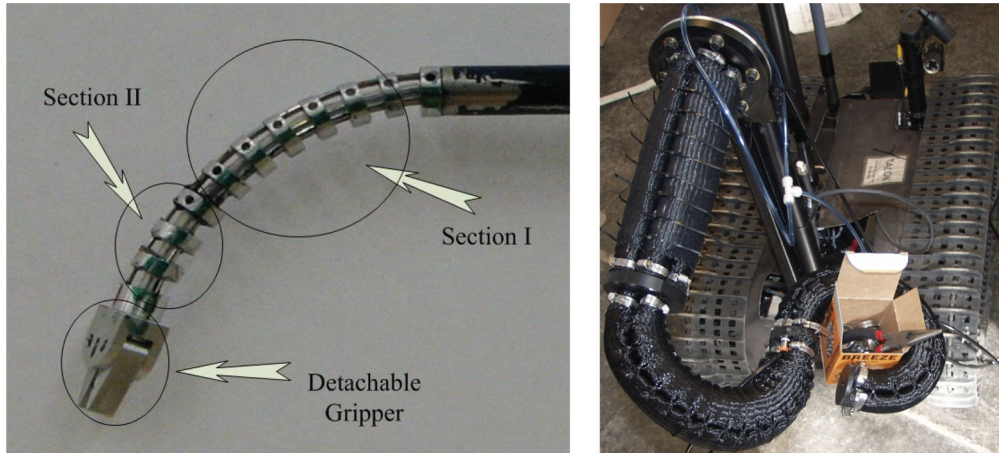


Fig. 7. Examples of flexible push-rod (left) and pneumatic (right) continuum robots with three actuators spaced at 120° radial intervals, whose kinematics are derived in Section 3.2.1. The 4.2-mm diameter multi-backbone robot by Xu and Simaan (2006) is designed for teleoperated surgery in the throat and airways. The OctArm robot (Jones and Walker 2006a) is mounted on a tracked, mobile base and actuated by latex rubber tubes, which are covered by a mesh which produces extension when pressurized. Left photo courtesy of Nabil Simaan, © 2006 IEEE. Right photo courtesy of Chris Rahn, © 2006 IEEE.

$$\begin{aligned} \hat{\mathbf{x}}_{\text{rot}} &= \begin{bmatrix} \hat{\mathbf{w}}_{\text{rot}} & \mathbf{v}_{\text{rot}} \\ 0 & 0 \end{bmatrix} = \begin{bmatrix} 0 & -1 & 0 & 0 \\ 1 & 0 & 0 & 0 \\ 0 & 0 & 0 & 0 \\ 0 & 0 & 0 & 0 \end{bmatrix} \quad \text{and} \\ \hat{\mathbf{x}}_{\text{inp}} &= \begin{bmatrix} \hat{\mathbf{w}}_{\text{inp}} & \mathbf{v}_{\text{inp}} \\ 0 & 0 \end{bmatrix} = \begin{bmatrix} 0 & 0 & \kappa & 0 \\ 0 & 0 & 0 & 0 \\ -\kappa & 0 & 0 & 1 \\ 0 & 0 & 0 & 0 \end{bmatrix}^T, \end{aligned} \quad (12)$$

where as shown, $\hat{\cdot}$ maps from \mathbb{R}^3 to $\mathfrak{so}(3)$ (the Lie algebra of $\text{SO}(3)$) and also from \mathbb{R}^6 to $\mathfrak{se}(3)$ (the Lie algebra of $\text{SE}(3)$), as used in Murray et al. (1994). Applying the product of exponentials formula yields

$$T = e^{(\hat{\mathbf{x}}_{\text{rot}}\phi)} e^{(\hat{\mathbf{x}}_{\text{inp}}\ell)}, \quad (13)$$

which is identical to (1) and evaluates to (2). Similarly, the single set of twist coordinates

$$\mathbf{x} = [0 \ 0 \ 1 \ -\kappa \sin \phi \ \kappa \cos \phi \ 0]^T \quad (14)$$

exponentiated as $e^{(\hat{\mathbf{x}}\ell)}$ yields (3).

3.1.6. Summary of Robot-independent Mapping. In summary, we have shown in this section that the derivation of a robot-independent mapping for the forward kinematics of a piecewise constant-curvature robot can be accomplished with a variety of approaches. Our primary purpose here was to show that many seemingly disparate approaches produce identical results (namely (2) and (3) when written in homogeneous matrix form) when placed in a common coordinate frame and stated using consistent symbols and mathematical terminology. While this may be clear to researchers experienced in the field, it is our experience that for

newcomers to continuum robotics, arriving at this conclusion requires significant effort and an intensive literature survey, which has led to some results being redemonstrated multiple times in the literature. It is our hope that this exposition will provide an easier entry into continuum robotics for new researchers, and also illustrate the diversity of approaches available to those pursuing extensions to basic constant-curvature theory, as discussed in Section 6.

3.2. Robot-specific Arc Parameter Mappings

The robot-independent mapping $\mathbf{f}_{\text{independent}}$ (see Figure 2) developed thus far results from the solution of a purely kinematic problem, namely that of mapping a piecewise constant-curvature arc described in configuration space (κ, ϕ, ℓ) to a task space position and orientation (\mathbf{x}) , which can be expressed as a homogeneous transformation matrix). In contrast, the robot-specific mapping $\mathbf{f}_{\text{specific}}$ maps from actuator or joint space (e.g. tendon lengths, pneumatic chamber pressures, etc.) to configuration space (κ, ϕ, ℓ) . This mapping is usually developed by examining the forces and moments applied by the actuators and transmitted through the structure of a continuum robot. Sometimes simplifying assumptions are introduced into this analysis, the most common being that constant moments are applied along the robot, implying (by Bernoulli–Euler beam mechanics) that it will assume a circular arc.

Because the manner in which actuators define arc parameters is generally unique to each actuation strategy, developing this mapping requires modeling of actuator–support structure interaction. In this section we provide several case studies for how the robot-specific mapping has been obtained for continuum robots with different actuation methods. Herein, we provide references to original source material, then present results (simplified where possible, and cast in the notation of this paper) for several common

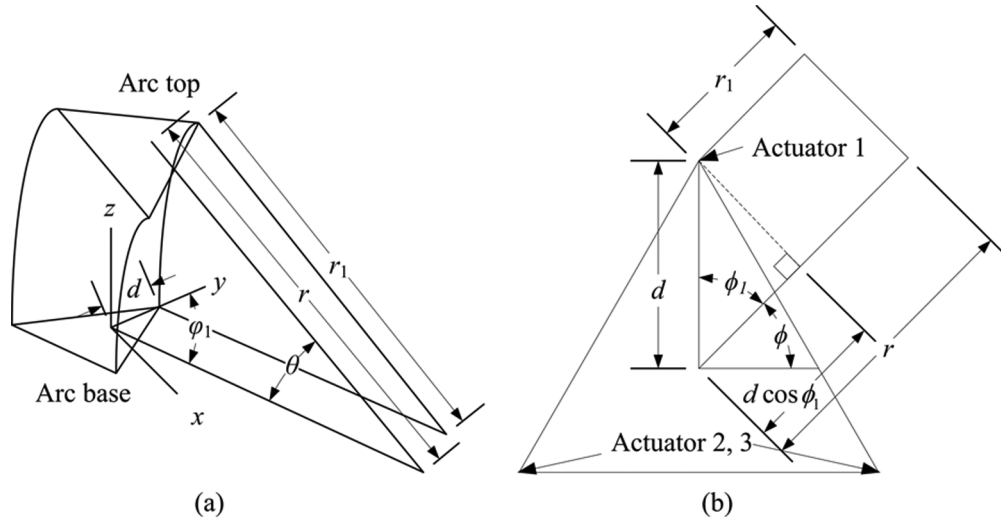


Fig. 8. (a) An illustration of an arc section in which various arc parameters are defined. (b) A diagram of the base section seen from above, from which (15) results.

continuum robot designs, which cover most of the actuation strategies currently in use.

3.2.1. Robots Shaped by Continuously Bending Actuators.

One common style of continuum robot construction (see, e.g., Chen et al. (2004), Jones and Walker (2006b), Ohno and Hirose (2001), and Bailly and Amirat (2005), and Xu and Simaan (2008), among others) is composed of actuators which bend continuously, such as flexible rods or pneumatic tubes. Figure 7 shows two realizations of such designs. A closed-form relationship between actuator lengths and the resulting shape is useful for real-time control which enables applications such as those discussed in Section 2.

Therefore, we seek to derive expressions for the arc parameters ($\ell(\mathbf{q})$, $\kappa(\mathbf{q})$, $\phi(\mathbf{q})$) for a single-section, three-actuator continuum robot, as a function $\mathbf{f}_{\text{specific}}$ (see Figure 2) of the “joint variables” $\mathbf{q} = [l_1 \ l_2 \ l_3]^T$ which describe the lengths of three pneumatic chambers or three flexible rods. What follows is a simplified version of derivations which can be found in Bailly and Amirat (2005) and Chen et al. (2005); Xu and Simaan (2008) provides an equivalent approach using a two-angle parametrization rather than the angle-curvature approach presented in this paper.

Figure 8(a) provides a view of the base and top of a single-section continuum robot, while Figure 8(b) shows the base of the same section viewed from above while looking down along the z -axis. As shown by the geometry in the figure, the radius of curvature r measured from the robot’s center relates to the radius of curvature for each individual actuator (denoted by $i \in 1 \dots 3$) according to

$$r_i = r - d \cos \phi_i, \quad (15)$$

where d is the distance from the center of a section of the robot to the center of the actuator (which is the same for all

actuators) and ϕ_i specifies the angle between the robot’s bending direction and the location of actuator i .

Multiplying (15) by the arc angle θ illustrated in Figure 8(b) and recalling that $\ell = \theta r$ and $l_i = \theta r_i$, the relationship between the arc length of the robot (ℓ) and the arc length of the i th actuator (l_i) is

$$\ell = l_i + \theta d \cos \phi_i. \quad (16)$$

Given this relationship, it is possible to determine $\ell(\mathbf{q})$ by noting that actuator locations (as shown in Figure 8) are related to the bending plane of the robot $\phi(\mathbf{q})$ by $\phi_1 = 90^\circ - \phi$, $\phi_2 = 210^\circ - \phi$, and $\phi_3 = 330^\circ - \phi$. Therefore, $\sum_{i=1}^3 \cos \phi_i = 0$. Thus, combining (16) from $i = 1 \dots 3$ yields

$$\ell(\mathbf{q}) = \frac{l_1 + l_2 + l_3}{3}. \quad (17)$$

Equation (16) determines $\phi(\mathbf{q})$ as follows. Applying (16) to the first two actuators and setting the right-hand sides equal yields $\theta d = (l_2 - l_1)/(\cos \phi_1 - \cos \phi_2)$. To obtain ϕ , apply the same procedure to actuators 2 and 3, equate the results, and insert the above-mentioned relationships between ϕ_i and ϕ to obtain

$$\phi(\mathbf{q}) = \tan^{-1} \left(\frac{\sqrt{3}(l_2 + l_3 - 2l_1)}{3(l_2 - l_3)} \right). \quad (18)$$

To obtain the curvature of the robot $\kappa(\mathbf{q})$, first recall that $\theta = \kappa \ell = l_i/r_i$, so that $r_i = l_i/\kappa \ell$, which when combined with (15) yields $\kappa = (\ell - l_i)/\ell d \cos \phi_i$. Considering a single actuator (e.g. $i = 1$ so that $\phi_1 = 90^\circ - \phi$) in (17) implies that $\kappa = (l_2 + l_3 - 2l_1)/((l_1 + l_2 + l_3) d \sin \phi)$. Combining this and (18) with the identity $\sin(\tan^{-1}(y/x)) = y/\sqrt{x^2 + y^2}$ and simplifying yields the desired result, namely,

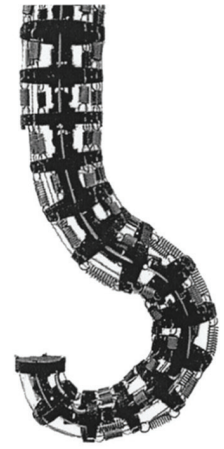
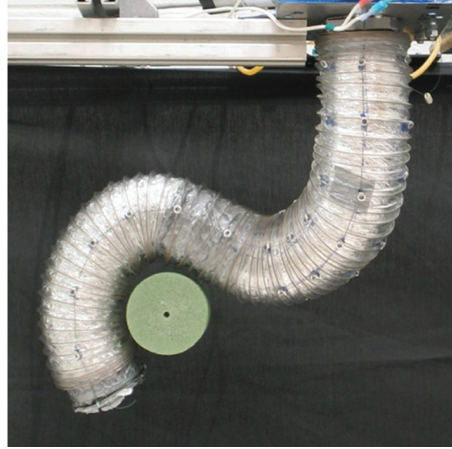
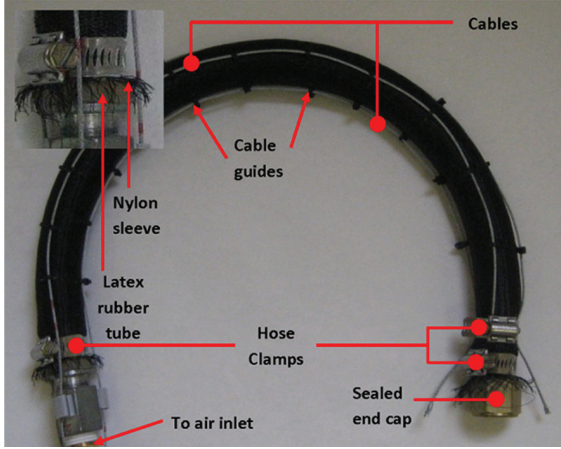


Fig. 9. Three examples of cable-driven robots. (Left) A latex rubber tube with three cables at 120° intervals creates an extensible wire-actuated continuum robot (Neppalli and Jones 2007). Copyright © 2007 IEEE. (Center) Similarly, the Air-OCTOR multi-section continuum robot consists of a pressurized hose around which cables are spaced at 120° intervals (Jones and Walker 2006a), © 2006 IEEE. (Right) The Clemson Elephant Trunk hyperredundant robot (Hannan and Walker 2003) consists of a series of U-joints with springs between jointed sections, producing an inextensible robot with approximately constant curvature within each section. Photo courtesy of Ian Walker, copyright © 1999 IEEE).

$$\kappa(\mathbf{q}) = \frac{2\sqrt{l_1^2 + l_2^2 + l_3^2 - l_1l_2 - l_1l_3 - l_2l_3}}{d(l_1 + l_2 + l_3)}. \quad (19)$$

In summary, Equations (17)–(19) give the robot-specific map $\mathbf{f}_{\text{specific}}$ from actuators to arc parameters $(\ell(\mathbf{q}), \kappa(\mathbf{q}), \phi(\mathbf{q}))$. The shape of the robot's section can then be obtained via the results given in Section 3.1. This framework also applies to multi-section robots; each section can be independently considered and will yield one set of arc parameters.

The kinematics for the four-actuator case can be considered in a similar manner to the three-actuator derivation above, although it has not specifically been articulated in this way in the literature as far as the authors are aware. For continuum robots with four actuators, $\phi_1 = \cos \phi$, $\phi_2 = \cos(90^\circ - \phi) = \sin \phi$, $\phi_3 = \cos(180^\circ - \phi) = -\cos \phi$, and $\phi_4 = \cos(270^\circ - \phi) = -\sin \phi$. Following the same steps as the three-actuator derivation above yields the desired result. Specifically, combining (16) from $i = 1 \dots 4$ yields

$$\ell(\mathbf{q}) = \frac{l_1 + l_2 + l_3 + l_4}{4}. \quad (20)$$

Similar to the three-actuator case, applying (16) to actuators 1 and 3, then setting the right-hand sides equal produces an expression which can be solved for θd . Repeating this for actuators 2 and 4 produces a second expression for θd . Equating the two and solving,

$$\phi(\mathbf{q}) = \tan^{-1} \left(\frac{l_4 - l_2}{l_3 - l_1} \right). \quad (21)$$

Again, following the three-actuator case, choosing $i = 2$ in $\kappa = (\ell - l_i)/\ell d \cos \phi_i$ then substituting (20) for ℓ gives an expression for κ in terms of $l_{1\dots 4}$ and ϕ . Substituting ϕ from

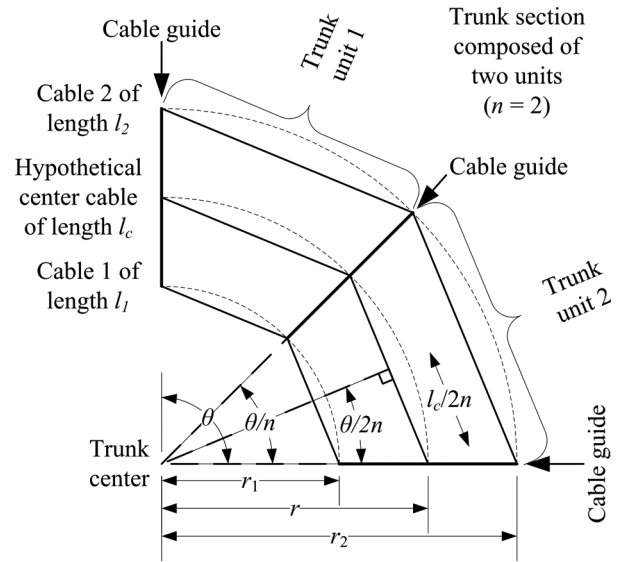


Fig. 10. Schematic of a single circular section of a cable-driven continuum robot. This section includes one cable guide (often there are several guides per section) that subdivides it into two units ($n = 2$). This two-dimensional, in-plane view omits one wire for simplicity and shows the special case where the bending plane happens to make the wires equidistant from the central backbone; however, results derived here also apply to general bending planes. The geometry presented shows that $\sin(\theta/2n) = (l_c/2n)/r$, producing (23).

(21) and simplifying,

$$\kappa(\mathbf{q}) = \frac{(l_1 - 3l_2 + l_3 + l_4)\sqrt{(l_4 - l_2)^2 + (l_3 - l_1)^2}}{d(l_1 + l_2 + l_3 + l_4)(l_4 - l_2)}, \quad (22)$$

which completes the derivation.

However, before we leave this topic, a few words are in order regarding the mechanical arrangement of some robots, particularly those actuated by push rods (Xu and Simaan 2006, Xu and Simaan 2008) that are over-actuated. Here, an additional inextensible central rod defines a constant length ℓ of each section of the robot. In this case, (17) shows that knowledge of two rod lengths l_1, l_2 defines the required length l_3 for the third rod, assuming all three rods bend with constant curvature. This kinematic over-determination is valuable: one can choose a redundancy resolution that minimizes the load on each backbone and thus reduces the risk of buckling (Simaan 2005). We also note that for wire-actuated robots, which may be either under- or over-actuated, additional complexities arise in constructing multi-section robots, due to coupling between cables which pass through multiple sections. The multi-section case is discussed in Section 4.

3.2.2. Robots Shaped by Tendons. A second frequently applied continuum robot design (see, e.g., Hannan and Walker (2003), Ciésłak and Morecki (1999), Jones and Walker (2006b), and Immega and Antonelli (1995)) utilizes three cables, as shown in Figure 9. Cable guides placed at equally spaced intervals along the robot cause its shape to approximate a circular arc, while dividing the cables into line segments which inscribe the arc formed by the robot. Measuring and controlling cable length then enables shape description and control based on the analytical relationships developed below.

One derivation for the forward kinematics of a single-section three-cable cable-driven continuum robot was provided in Jones and Walker (2006a). Here we contribute a simplified derivation, which is similar to that described in the previous section for robots shaped by continuously bending actuators. As in the previous section, this procedure can then be repeated to derive four-cable kinematics.

Here, we assume that cables travel in a straight line from one cable guide to the next in a uniformly bending section of the robot, subdividing each section into n units that begin and end at the $n + 1$ cable guides as shown in Figure 10. Examining one unit of an n -unit section, note that Equation (15) applies where r_i now specifies the radius of curvature of a circle into which line segments (defined by cables of length l_i passing from cable guide to cable guide) can be inscribed as illustrated in Figure 10. Likewise, r gives the radius of a circle into which a hypothetical cable of length l_c , which passes through the center of each segment, can be inscribed.

As shown in Figure 10, a unit of radius $r = \kappa^{-1}$ which bends through θ/n radians (where $\theta = \kappa s$) produces a cable length

$$l_c = 2nr \sin(\theta/2n). \quad (23)$$

Again referring to the figure, the same principle also applies to the per-cable lengths and radii, so that $l_i = 2nr_i \sin(\theta/2n)$. Multiplying (15) by $2n \sin(\theta/2n)$,

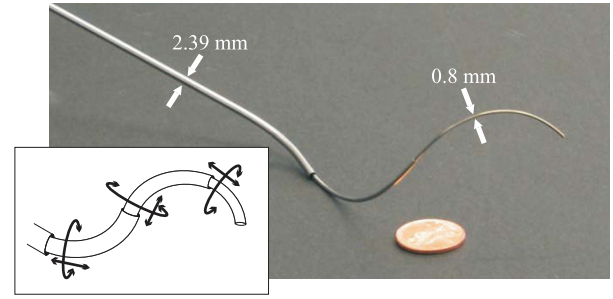


Fig. 11. A three-tube active cannula with inset line drawing showing degrees of freedom (Webster et al. 2009), © 2009 IEEE.

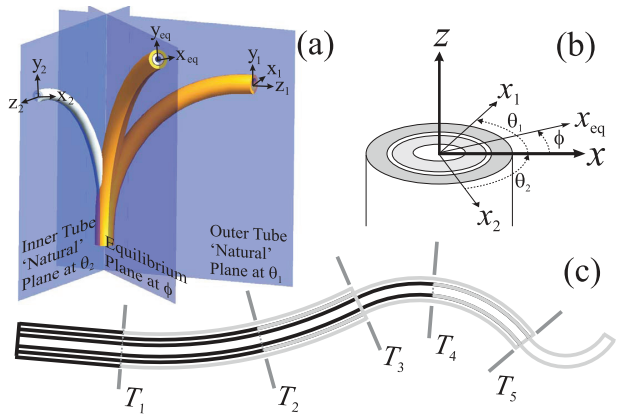


Fig. 12. (a) When two circularly precurved tubes are placed concentrically and rotated at their bases, their resultant shape can be approximated by a circular arc lying in a plane between the tubes' individual planes. (b) Cross section showing tube individual frames and equilibrium frame. (c) An active cannula consists of $2n$ such sections for n tubes: black lines denote straight tube segments while gray lines denote circularly precurved tube segments. Images adapted from Webster et al. (2009), original source © 2009 IEEE.

substituting, and solving gives

$$l_c = l_i + d2n \sin(\theta/2n) \cos \phi_i. \quad (24)$$

In the same manner as the continuously bending actuator case in (17), combining (24) over all three actuators produces

$$l_c = \frac{l_1 + l_2 + l_3}{3}. \quad (25)$$

By the same reasoning, one can apply (24) to two cables and equate the results to yield $d2n \sin(\theta/2n) = (l_2 - l_1)/(\cos \phi_1 - \cos \phi_2)$. The same procedure can then be applied to the second and third cables. Equating and solving gives (18).

The derivation for $\kappa(\mathbf{q})$ is also similar to the procedure described for continuously bending actuation, and yields the same result. This can be derived from (23) and following, which yield $\sin(\theta/2n) = l_c/2nr = l_i/2nr_i$, implying that $r_i = l_i/\kappa l_c$. Equating this with (15) and solving, we obtain $\kappa = (l_c - l_i)/l_c d \cos(\phi_i)$. Choosing $i = 1$ so that $\phi_i = 90^\circ - \phi$ and substituting (25) yields

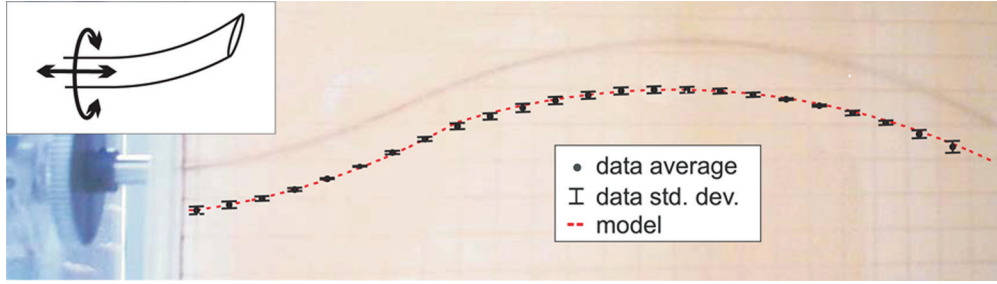


Fig. 13. Photo of a steerable needle inserted into simulated muscle, with model prediction superimposed and offset below the needle, so that the needle can be seen.

$\kappa = (l_2 + l_3 - 2l_1)/(l_1 + l_2 + l_3)d \sin \phi$. The remainder of the derivation is then identical to the pneumatic case and yields (19).

The arc length of the robot $\ell(\mathbf{q})$ can be determined from (23), which yields $\ell = (2n/\kappa) \sin^{-1}(l_c \kappa/2n)$. Applying (19) and (25) yields

$$\ell(\mathbf{q}) = \frac{nd(l_1 + l_2 + l_3)}{2\sqrt{l_1^2 + l_2^2 + l_3^2 - l_1l_2 - l_1l_3 - l_2l_3}} \sin^{-1} \left(\frac{\sqrt{l_1^2 + l_2^2 + l_3^2 - l_1l_2 - l_1l_3 - l_2l_3}}{3nd} \right). \quad (26)$$

In summary, the expressions for $\kappa(\mathbf{q})$ in (19) and $\phi(\mathbf{q})$ in (18) for tendon-driven continuum robots are identical to those for the robots with continuously bending actuation described in the previous section. Therefore, (18), (19), and (26) define $\mathbf{f}_{\text{specific}}$ for these robots. The only difference between the two types, arising from the fact that wires go straight between support disks rather than through curved paths, is in the arc length parameter $\ell(\mathbf{q})$ in (26). The four-actuator case follows similarly. Imitating the procedure above but using actuators 1, 3 and 2, 4 as in the continuously bending actuation case yields $\phi(\mathbf{q})$ in (21) and $\kappa(\mathbf{q})$ in (22). Applying (26) with these updated formulas for ϕ and κ then produces $\ell(\mathbf{q})$. See Hannan and Walker (2003) for an alternate derivation.

The inextensibility of many cable-driven robots such as those of Buckingham (2002), Hannan and Walker (2003) and Ciésłak and Morecki (1999), leads to an over-actuated system. Similar to the previous section, (25) prescribes one of the cable lengths when the other two are known, assuming the robot retains a constant-curvature shape. However, additional difficulties arise due to cable extension resulting from loading, which requires examination of the statics of the continuum robot and the resulting forces applied to its cables to properly regulate cable tension, avoid cable slack, and address both under- and over-actuation in these systems (Camarillo et al. 2008, 2009a). Section 4.2 treats these problems in the more challenging context of a multi-section robot.

3.2.3. Concentric Tube Continuum Robots. Concentric tube continuum robots, also known as active cannulas due

to their potential medical applications (Figure 11), are a relatively new type of continuum robot (Sears and Dupont 2006; Webster et al. 2006b; Sears and Dupont 2007; Rucker and Webster 2009b; Webster et al. 2009; Dupont et al. 2010; Rucker et al. 2010a, b). A distinguishing characteristic of the active cannula design (aside from its small diameter) is that bending actuation is built into the backbone, which is composed of telescoping, precurved elastic tubes. These can be rotated and translated with respect to one another to transmit bending moments.

The joint variables for an active cannula are the translations (r) and rotations (q) of component tubes. Thus, joint space consists of $\mathbf{q} = [\rho_1 \ \theta_1 \ \cdots \ \rho_n \ \theta_n]^T$. Neglecting torsion, actuators at tube bases directly specify tube axial rotation angles at all points along the active cannula.¹ Under this assumption and with circular curvature preformed into each component tube, the active cannula consists of piecewise constant-curvature links (Webster et al. 2006b; Sears and Dupont 2006; Webster et al. 2009) as shown in Figure 12. To determine the arc parameters of a given link, one can apply Bernoulli–Euler beam mechanics. For a collection of tubes with circular precurvatures k_i and a deformed resultant circular curvature common to all tubes κ , moments will be constant along the length of each tube in a given section and can be described by $\kappa - k_i = M/EI$, where M is the bending moment, E is the elastic modulus, and I is the cross-sectional inertia of the tube. Writing a moment balance in the equilibrium coordinate frame in component form, one can obtain curvature components of

$$\kappa_x = \frac{\sum_{i=1}^n E_i I_i k_i \cos \theta_i}{\sum_{i=1}^n E_i I_i}, \quad \kappa_y = \frac{\sum_{i=1}^n E_i I_i k_i \sin \theta_i}{\sum_{i=1}^n E_i I_i}, \quad (27)$$

where θ_i are the angles input at the base of the link. These can be converted into arc parameters by observing that the equilibrium plane and curvature are

$$\phi(\mathbf{q}) = \tan^{-1} \left(\frac{\kappa_y}{\kappa_x} \right) \quad \text{and} \quad \kappa(\mathbf{q}) = \sqrt{\kappa_x^2 + \kappa_y^2}, \quad (28)$$

which defines $\mathbf{f}_{\text{specific}}$ for this type of continuum robot.

Tube transition points (points where tubes either end or transition from straight to curved) bound each link in an active cannula, and together with actuator displacements directly define link lengths through straightforward linear algebraic relationships. The exact functions depend on the order of transition points, and examples and methods for calculation of link lengths are given in Webster et al. (2009) and Sears and Dupont (2006).

3.2.4. The Steerable Needle. Needles can be “steered” (guided through curved trajectories) inside soft tissue in a variety of ways (for an overview, see Webster (2007)). One means of steering needles is to make the needle shaft flexible (e.g. use a material such as Nitinol) and harness the asymmetric forces of a beveled tip. Work in Webster et al. (2006a) shows that the trajectory of such a bevel-steered needle can be modeled as having piecewise constant curvature. Curves begin and end when the needle is rotated axially, redirecting the bevel and thus the direction of forward progression. A distinguishing feature of bevel steering is that the backbone (needle shaft) can have as many arcs as desired (a new one begins with each bevel reorientation), and with constant axial rotation during insertion steerable needles can also achieve helical trajectories. However, in contrast to other continuum robots, only arcs forward of the current tip position can be affected by the actuators. Arcs embedded in tissue will stay in place with constant arc parameters, regardless of actuator motion, because they are held by the tissue (Webster et al. 2005). When retracted, the needle will return along the path through which it entered the tissue.

Steerable needle kinematics can be described by considering body velocity. The body frame twist coordinates corresponding to insertion and rotation of the needle are the same as those given in (10)–(11), namely,²

$$\mathbf{x}_{\text{rotation}} = [0 \ 0 \ 0 \ 0 \ 0 \ 1]^T \text{ and}$$

$$\mathbf{x}_{\text{insertion}} = [0 \ 0 \ 1 \ 0 \ \kappa \ 0]^T.$$

Converting these to twists, we have

$$\hat{\mathbf{x}}_{\text{insertion}} = \begin{bmatrix} \kappa \hat{\mathbf{e}}_2 & \mathbf{e}_3 \\ 0 & 0 \end{bmatrix} \quad \hat{\xi}_{\text{rotation}} = \begin{bmatrix} \hat{\mathbf{e}}_3 & 0 \\ 0 & 0 \end{bmatrix}, \quad (29)$$

where \mathbf{e}_i are standard basis vectors and the $\hat{\cdot}$ notation is used as in (12).

If the sequence (and distances) of insertion and rotation motions for a complete needle trajectory are known *a priori*, the product of exponentials formula can be applied directly in a similar manner to (13), as $T = e^{(\hat{\mathbf{x}}_{\text{insertion}} \ell_1)} e^{(\hat{\xi}_{\text{rotation}} \phi_1)} \dots e^{(\hat{\mathbf{x}}_{\text{insertion}} \ell_n)} e^{(\hat{\xi}_{\text{rotation}} \phi_n)}$.³ However, normally the input degrees of freedom will be dynamically manipulated by a control system, in which case the forward translation of the needle will be given by

$$\dot{T}(t) = T(t)(u_1 \hat{\mathbf{x}}_{\text{insertion}} + u_2 \hat{\xi}_{\text{rotation}}), \quad (30)$$

where u_1 and u_2 are the insertion and rotation velocity

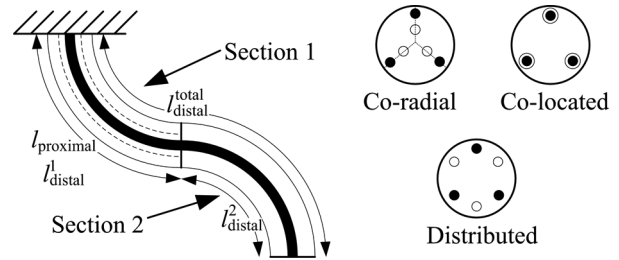


Fig. 14. A two-section robot illustrates the “tangle/untangle” process. Co-located concentric proximal and distal actuators (as is the case with the flexible push-rod design: the sketch above indicates actuators that pass directly through one another) simplify the process because the section lengths of all rods, both those that actuate the base and tip section, passing through the base section are identical. When cables for multiple sections lie at equal angles about the central axis of the device (termed “co-radial” above), a slightly more complex process of mapping outer actuator lengths to shape, and then back to inner actuator lengths, decouples the actuator lengths. In the most complex case for multi-section cable-driven designs, where the cables for proximal and distal sections cannot be coaxial (and are therefore distributed around the edge of each disk), an iterative procedure known as tangle/untangle (Jones and Walker 2006b) or a statics model with optimization (Camarillo et al. 2009a) can be used to determine multi-section cable lengths.

inputs, respectively, applied at the needle base. When the needle is used under closed-loop control with feedback from a medical imaging system, a needle controller (see, e.g., Kallam and Cowan (2009)) determines u_1 and u_2 in real-time and applies them using motors connected to the needle base (see Webster et al. (2005) and Reed et al. (2008)). To determine needle pose, (30) can be integrated (see Webster et al. (2006a) for details and Park and Chung (2005) for an in-depth discussion on several numerical integration techniques) to determine needle pose.

4. Multi-section Forward and Inverse Kinematics

4.1. Forward Kinematics

Many continuum robot applications require multi-section robots, in order to provide a sufficient number of DOF for task requirements. Since a single section generally provides two or three DOF, positioning the robot’s tip with six DOF requires a minimum of two to three sections, and more are desirable to increase workspace size and provide redundant solutions. Actuator length limits can also constrain single-section robot motion to a subspace of the theoretical workspace, producing a relatively small workspace for many single-section manipulators (see Jones and Walker (2006b) for one example). Furthermore, whole-arm grasping and the ability to work in cluttered environments often require one or more sections dedicated to the task, while other sections toward the robot’s base support and position distal sections. All of these factors provide ample motivation for multi-section robots; indeed, many of the existing

designs listed in Table 1 are equipped with multiple sections.

However, multi-section continuum robots can introduce additional complexity in the mappings illustrated in Figure 2. In general, the robot-independent forward kinematic results are straightforward to generalize to the multi-section case. One simple way to see this is to consider each section as having its own transformation (Equations (1) or (2) when expressed using the homogeneous matrix representation), then simply multiplying these transformations as one would for traditional serial robot link transformations. However, the robot-specific mapping cannot always be so cleanly decoupled, and doing so sometimes requires consideration of the whole robot and simultaneous solution of all sections.

In terms of the example designs given in Section 3.2, the cables and push-rods that actuate distal sections of the robot (those toward the robot's tip) pass through and therefore affect the shape of proximal sections, requiring a whole-robot solution. In contrast, the latex rubber tubes in pneumatically actuated robots terminate at each section boundary, producing a mechanically decoupled design solvable on a per-section basis. While distal sections in concentric-tube continuum robots also pass through proximal sections and affect their shape, this coupling is directly built into the model as expressed in Section 3.2.3. For the steerable needle, there is no coupling, and each section in an *a priori* determined actuator trajectory does not affect other sections.

Thus, the designs where extension to multiple sections requires additional analysis are those involving push rods and cables. Referring to Figure 14, co-located actuators provide a straightforward method to determine distal actuator length as the sum of all co-located proximal actuators. For example, the robot in Xu and Simaan (2008) features hollow push rods, in which distal rods lie inside proximal rods. In the more common case of distributed actuation, the length of a distal actuator must be computed by referring to the arc parameters for proximal sections then using a single-section mapping to compute these lengths as they pass through each proximal section, a process termed "tangle/untangle" in Jones and Walker (2006b). If actuator forces cause compression of the robot and extension of the actuating cables, a consideration of statics can enable calculation of cable lengths (Camarillo et al. 2009a).

4.2. Inverse Kinematics

As with all serial robots, and particularly in the case of redundant robots, inverse kinematics is challenging. For a constant-curvature continuum robot, one usually begins by computing the inverse mapping between task space and configuration space (the robot-independent inverse mapping). This produces the arc parameters of all sections of the robot, which correspond to the desired tip pose. Computing all possible solutions to this problem for a continuum robot with a large number of sections is clearly not trivial, but several approaches for inverse kinematics do

exist. A closed-form geometric approach is given for single and multiple sections in Neppalli et al. (2009), based on modeling each section using a spherical joint and a straight rigid link, then applying an analytical process to solve inverse kinematics for this model before converting back to arc parameters. This approach provides simple access to the entire solution space of the rigid-link robot and can easily be applied to an n -link robot. However, this formulation does not yet account for physical actuation limits, such as limited actuator lengths, forces, or locations.

The Jacobian (see Section 5.1) provides another approach to robot-independent inverse kinematics. It finds a single solution to the problem by servoing a virtual copy of the robot from any initial guess (including the robot's current configuration) to the desired configuration (see, e.g., Sears and Dupont (2007) and Webster et al. (2008) for active cannula results). In this Jacobian-based inverse kinematics strategy, it is possible to build actuator limits into the control law so that the robot's trajectory is always physically realizable.

The inverse mapping from arc parameters to actuator parameters differs for each kind of continuum robot, similar to the forward mapping. Bevel-steered needle inverse kinematics are the most straightforward, since the desired ϕ for each section directly defines the amount of axial rotation necessary after each forward translation along the previous section. Inverse kinematics of concentric-tube continuum robots are only slightly more complex, given a set of arc parameters in their workspace. For these robots, one can work backward from the distal section (see Figure 12), where ϕ_n is equivalent to the axial angle of the single tube it contains. The second-to-last section contains two tubes, so given its arc parameters and the fact that we have already determined the axial angle of one of the two tubes it contains, Equations (27) and (28) have only one unknown, and can be solved in closed form for a second axial tube angle. Repeating this procedure for each subsequent section as one moves toward the robot's base, one tube angle is completely defined by each section.

Additional single-section inverse mappings from arc parameters to actuator parameters include derivations for push rod-actuated robots (Xu and Simaan 2008) and for single-section cable and pneumatically actuated robots (Jones and Walker 2006a). Using these mappings, Jones and Walker (2006b) produced an analytical derivation of the workspace of these robots under actuator length limit constraints and describes a "tangle/untangle" algorithm for multi-section cable-actuated robots with actuators equally spaced about the base of the trunk.

The above algorithms restrict their attention to constant-curvature kinematics, and thus do not include real-world effects that can be important in some continuum robot designs, such as gravitational loading or friction. For example, friction can cause non-circular deformation in the flexible push-rod design. Fortunately, this can be overcome by compensation that makes use of redundant actuation in the single- (Xu and Simaan 2006) and multi-section cases

(Simaan et al. 2009). Likewise, some continuum robot designs undergo appreciable axial compression due to actuator forces, necessitating a static analysis of the system to compute cable lengths which correspond to desired arc parameters (Camarillo et al. 2009a).

5. Differential Kinematics

One approach to derive the Jacobian matrix for a continuum robot is to compute the full kinematics as described in Section 3 using both the system-specific and system-independent mappings, then to directly differentiate the components of the resulting homogeneous transformation (see, e.g., Jones and Walker (2006a) and Hannan and Walker (2003)). While this is conceptually straightforward, in practice it can become computationally cumbersome. A multi-section robot would require multiplication of several copies of (2) or (3) and substitution of potentially lengthy robot-specific definitions of arc parameters, such as those derived in Section 3.2.

However, a robot-specific/robot-independent approach similar to that taken with forward kinematics earlier in this paper can also be applied to differential kinematics (Webster et al. 2008). To accomplish this, first observe that forward kinematics is a composition of maps, namely $T = T(\kappa(\mathbf{q}), \phi(\mathbf{q}), \ell(\mathbf{q}))$. This implies that we can use the chain rule to compute differential kinematics.

5.1. Robot-independent Jacobian

At first glance, applying the chain rule to (13) is not straightforward, because both $\kappa(\mathbf{q})$ and $\ell(\mathbf{q})$ appear in the second exponential. However, following (Webster et al. 2008), we begin by computing spatial velocity for one section (the j^{th} section) of a continuum robot as

$$\hat{V}_j^s = \dot{T}_j T_j^{-1} = \hat{e}_6 \Delta \dot{\phi}_j + e^{\hat{e}_6 \Delta \phi_j} \left(\frac{d}{dt} e^{(\hat{e}_3 + \hat{e}_4 \kappa_j) \ell_j} \right) T_j^{-1}, \quad (31)$$

where T_j is given in (13) but with ϕ_j replaced with $\Delta \phi_j = \phi_j - \phi_{j-1}$ to enable the result to be used with a multi-section robot. Using trigonometric series it can be shown that the final term of (31) reduces to $e^{\hat{e}_6 \Delta \phi_j} \hat{A}_j e^{-\hat{e}_6 \Delta \phi_j}$, where

$$\hat{A}_j = \begin{bmatrix} \hat{e}_2 \dot{\kappa}_j \ell_j \left(\dot{\ell}_j + \frac{\dot{\kappa}_j (\kappa_j \ell_j - \sin(\kappa_j \ell_j))}{\kappa_j^2} \right) \mathbf{e}_3 + \frac{\dot{\kappa}_j (\cos(\kappa_j \ell_j) - 1)}{\kappa_j^2} \mathbf{e}_1 \\ 0 \quad 0 \end{bmatrix}.$$

Converting (31) from $\text{se}(3)$ to \mathbb{R}^6 yields $V_j^s = \mathbf{e}_6 \Delta \dot{\phi}_j + \text{Ad}_{\hat{e}_6 \Delta \phi_j} \hat{A}_j$, which reduces to

$$V_j^s = \underbrace{\begin{bmatrix} \cos \Delta \phi_j (\cos(\kappa_j \ell_j) - 1)/\kappa_j^2 & 0 & 0 \\ \sin \Delta \phi_j (\cos(\kappa_j \ell_j) - 1)/\kappa_j^2 & 0 & 0 \\ -(\sin(\kappa_j \ell_j) - \kappa_j \ell_j)/\kappa_j^2 & 0 & 1 \\ -\ell_j \sin \Delta \phi_j & 0 & -\kappa_j \sin \Delta \phi_j \\ \ell_j \cos \Delta \phi_j & 0 & \kappa_j \cos \Delta \phi_j \\ 0 & 1 & 0 \end{bmatrix}}_{J_j^s} \begin{bmatrix} \dot{\kappa}_j \\ \Delta \dot{\phi}_j \\ \dot{\ell}_j \end{bmatrix}. \quad (32)$$

Note that J_j^s is well defined for all $(\kappa_j, \Delta \phi_j, \ell_j)$, even in the limit as κ_j approaches 0.

Given this single-section Jacobian, one can generalize to multiple sections by expressing individual section Jacobians in the spatial frame. Applying the relevant adjoint transformations,

$$J_{\text{robot}}^s = [J_0 \text{Ad}_{T_0} J_1 \text{Ad}_{T_{01}} J_2 \cdots \text{Ad}_{T_{0(m-1)}} J_m] \quad (33)$$

where J_j is the j^{th} section Jacobian (32), and $T_{0j} = T_0 T_1 \cdots T_j$. This result can then be used to determine the spatial velocity (see Murray et al. (1994) for an in-depth discussion of the proper interpretation of spatial and body velocities) of the tool frame by multiplying it on its right by a vector consisting of a stack of all m triplets of arc parameter velocities.

5.2. Robot-specific Derivatives

Some continuum robots permit direct control of arc parameters. With such robots, the robot-independent result above can be applied directly. In others, including some of our examples in Section 3.2, the mapping between joint variables and arc parameters may be written in closed form (see, e.g., Bailly and Amirat (2005), Jones and Walker (2006a), and Sears and Dupont (2007)). When this is possible, one can directly differentiate the expressions for the arc parameters. In still other cases, including active cannulas when they are approximated as piecewise constant curvature, with torsion modeled in straight sections only as in Webster et al. (2009), obtaining arc parameters requires numerical energy minimization. Even this does not necessarily preclude a closed-form Jacobian. It has been shown in Webster et al. (2008) that by applying a local version of the implicit function theorem, one can arrive at a closed-form Jacobian for an active cannula. Efficient methods for obtaining the Jacobian for non-circular continuum robots, including piecewise constant-curvature robots of all designs under significant external loading (as well as active cannulas with variable precurvature and/or under external loading (Rucker et al. 2010a)) is an open research question that is discussed below in terms of future challenges in the field of continuum robots.

6. Opportunities For Future Research

The efforts of many researchers have led to significant advancements in the design, application, and theoretical foundation for continuum robotics, as has been reviewed in previous sections of this paper. However, before continuum robots become as pervasive as their rigid-link counterparts, a number of ongoing research challenges must be addressed. Here, we discuss several of the many themes that will be important in the future of continuum robotics research.

6.1. Design

The diversity of applications and sizes of continuum robots provide fertile ground for design innovation, as can be clearly seen from the examples in Section 2. The coupling of actuation and elastic support structure is an active area of research, as are the tradeoffs between distributed, discrete, and remote (e.g. cable) actuation, and the best combinations of these strategies. Related to this are the challenges of concatenating multiple sections (the actuators for distal sections can often influence the shape of proximal ones as described in Section 4.2), appropriately tuning or controlling overall robot stiffness to match application objectives, and identifying and using robust materials with long functional lifetimes. Similarly, it is not always clear how to incorporate actuator or structural limits (see, e.g., Jones et al. (2006)) into models to prevent robot self-damage or damage under load. Furthermore, many of the continuum robots developed to date have not yet been fitted with end-effectors. Depending on design, weight, and actuation, these end-effectors may require mechanical or algorithmic compensation for their effect on robot shape. Each of the above factors provide researchers with many opportunities for innovation in continuum robot design when approaching each new application.

6.2. Static Modeling

As we have described in this paper, the piecewise constant-curvature approximation is often useful and has been widely applied. However, general methods to characterize the error induced by this assumption do not currently exist. The common approach to justify the assumption is to (1) photograph the robot and observe that a circle fits the actual backbone shape “rather well”, (2) proceed with the subject matter of the paper (design, kinematics, application requirements, etc.), (3) experimentally assess overall performance of the entire robot system, and (4) conclude that if the experiments were successful then the piecewise constant-curvature approximation was sufficiently accurate. This process does not provide an early means of testing a single section of the robot to extrapolate whether a multi-section robot will be likely to meet design requirements. Thus, general results on error propagation based on metrics for the circularity (or lack thereof) of the physical robot shape would be valuable. Furthermore, in cases where piecewise constant curvature is not sufficient,

advancements will be needed in working with more complex variable curvature models. There is a great deal of current interest in obtaining deeper understanding of the fundamental mechanics of continuum robots in terms of general theories of elasticity, and both energy minimization (see, e.g., Rucker et al. (2010b), among others) and Cosserat rod theory (see, e.g., Trivedi et al. (2008a), Dupont et al. (2010), and Rucker et al. (2010a), among others) have yielded useful recent results. The ability to include the effects of gravity, torsion, and external loading in such models is particularly useful. Based on the current trajectory of this area of research, it appears likely that advancements will first come in the form of general models that account for these effects, and researchers will then seek parsimonious simplifications that capture salient features and are sufficiently accurate and efficient for use in real-time control.

6.3. Dynamic Modeling

In this paper we have reviewed static modeling results for constant-curvature robots. A particularly challenging emerging area of research involves deriving and practically applying dynamic models of continuum robots in a numerically stable form amenable to real-time implementation. The dynamic equations of continuum robots under various assumptions have been derived in the planar case (Gravagne et al. 2003; Tatlicioglu et al. 2007) and derivations based on an energy–work relationship (Ivanescu et al. 2007), conservation laws (Chirikjian 1995), and a Newtonian formulation of Cosserat rods (Trivedi et al. 2008a) exist. We note that some of the earliest, yet most advanced work in terms of practical implementation is that of Chirikjian (1995), where a variable geometry truss provided a means of computing planar continuum robot dynamics rapidly. We note also that several non-robotic applications of Cosserat rod dynamics address these issues (Spillmann and Teschner 2007; Lang et al. 2009) and show promise for future application in continuum robotics. In summary, efficient implementation of dynamic models for various kinds of continuum robots is an open and active area of research. It is likely that over the next few years dynamic models will become increasingly more general (many existing formulations are done in two dimensions and/or assume constant curvature), and that increasingly efficient and stable numerical techniques for real-time implementation will be developed, both of which facilitate the practical application of continuum robots in dynamic environments that require rapid motion.

6.4. Sensing, Control, and Calibration

Traditional encoders are not generally sufficient for determining continuum robot shape, since continuum robots have an infinite number of DOFs (they bend continuously). However, feedback on robot shape is necessary to enable closed-loop control. This has lead several researchers to explore computer vision for shape sensing (see, e.g.,

Chitrakaran et al. (2007), Camarillo et al. (2009b), and Croom et al. (2010)) and visual servo control. Developing imaging methods that are both accurate and efficient will be a key to real-time control. Control advancements may include methods of servoing the entire shape of the robot curve to a desired curve. Promising sensing possibilities other than computer vision include embedded strain gages or fiber optic techniques such as ShapeTape (see <http://www.measurand.com/>), while medical systems will likely employ intraoperative medical imaging. Such medical imaging may be similar to optical cameras (e.g. biplane fluoroscopy), or provide direct three-dimensional information (e.g. three-dimensional ultrasound (Burdette et al. 2010)). We note also that in addition to control, sensors can be used for robot calibration, enabling fitting of imprecisely known robot parameters (e.g. stiffnesses, lengths, etc.) to experimental data. This can be done in a variety of ways with many different sensors and continuum robot types, and Webster et al. (2009) and Xu and Simaan (2008) provide two specific examples this technique.

6.5. Complete Systems

Complete integrated systems are likely to include user interfaces and must address efficiency in order to implement the computations relating to robot motion in real time (see, e.g., Jones and Walker (2006b)). It is not yet clear what the optimal kinematic mappings between human user input and the curve of a continuum robot will be, although some promising initial studies have been done (see, e.g., Csencsits et al. (2005) and Immega and Antonelli (1995)). With regard to efficiency, deriving closed-form inverse kinematics (see, e.g., Neppalli et al. (2009), Rucker et al. (2009), and Sears and Dupont (2007)) may provide an alternative to Jacobian-based techniques, and one must also address limiting cases in a computationally robust way (Jones and Walker 2007). Furthermore, advancements are needed in motion planning and obstacle avoidance for continuum robots (see Lyons et al. (2009) for one approach). We also note that these topics have been addressed for hyperredundant robots (see, e.g., Hannan and Walker (2003) and Choset and Henning (1999)). Continuum robots also offer the possibility to manipulate objects with the whole arm (Mochiyama et al. 1999; Braganza et al. 2006), which can help the robot to securely grasp objects whose geometry or position is imprecisely known. In medical applications complete systems will include use of preoperative and intraoperative image data, statistical information about anatomical geometry, appropriate and interchangeable end-effectors, human interfaces, and assistance that can be provided to the doctor in the form of virtual fixtures (Kapoor 2007).

7. Conclusion

Continuum robots have been adopted in a wide variety of applications, as discussed in Section 2, and are becoming increasingly valuable tools for the robotics community.

Precisely because their most useful characteristics (dexterity in cluttered and unstructured environments, gentle and compliant interaction with objects, etc.) differ from those of traditional robots (rigidity, precision, suitability for highly structured environments), they require corresponding advancements in robotics theory. As reviewed in this paper, the most general models describing continuum robot shape (forward kinematics) involve numerical integration. Thus, in order to achieve closed-form results and thus facilitate real-time control, differential kinematics, inverse kinematics, etc., many researchers have applied the closed-form piecewise constant-curvature approximation and found it to be sufficiently accurate for their objectives.

Herein, we have reviewed many mechanical continuum robot architectures for which the piecewise constant-curvature approximation has been found to be applicable. Further, we have described important results in piecewise constant-curvature kinematics, setting them in a single coordinate frame and notational convention and indicating which results are robot-specific and which are robot-independent. The latter may be applied directly to each new (approximately) piecewise constant-curvature continuum robot design developed in the future.

In summary, continuum robots offer the potential to extend the benefits of robotics to applications that have not previously been approachable with robots. These include working in unstructured or constrained environments and manipulating delicate objects or those with imprecisely known shapes or locations. The study of continuum robotics is entering an exciting era. While useful general results such as those reviewed in this paper have been developed, there remain many avenues for future research and many promising new applications that have not yet been explored. Given the accelerating pace of fundamental progress in design, modeling, and practical implementation, continuum robots appear poised to become increasingly useful tools that will play key roles in the future of robotics.

Notes

1. Note that when torsion is included the shape of an active cannula becomes a general curve, as described by Rucker and Webster (2008, 2009a,b), Rucker et al. (2010b), and Dupont et al. (2009, 2010), although closed-form solutions are still possible in some cases. This is also true when external forces and moments are applied (Rucker et al. 2010a).
2. Note that the insertion twist given here is slightly different than the $\xi_{\text{insertion}} = [0 \ 0 \ 1 \ \kappa \ 0 \ 0]^T$ given in Webster III et al. (2006a) to be consistent with the frame convention used throughout this paper.
3. The order of exponentials within each pair describing a section is reversed here, with respect to (13), because the axial rotation at the end of the i th link affects the plane of link $i + 1$.

Acknowledgments

This work was funded in part by the National Science Foundation under grant # 0651803 and by Vanderbilt and Mississippi State Universities.

References

- Anderson, V. and Horn, R. (1967). Tensor arm manipulator design. *ASME Transactions*, **67-DE-57**(2): 1–12.
- Anderson, V. and Horn, R. (1970). Tensor arm manipulator. U.S. Patent 3,497,083.
- Andersson, S. B. (2008). Discretization of a continuous curve. *IEEE Transactions on Robotics*, **24**(2): 456–461.
- Antman, S. S. (2005). *Nonlinear Problems of Elasticity*, (Applied Mathematical Sciences, Vol. 107) (2nd edition). New York, NY, Springer.
- Aoki, T., Ochiai, A. and Hirose, S. (2004). Study on slime robot: development of the mobile robot prototype model using bridle bellows. *IEEE International Conference on Robotics and Automation*, Vol. 3, pp. 2808–2813.
- Aoki, T., Ohno, H. and Hirose, S. (2002). Design of slim slime robot II (SSR-II) with bridle bellows. *IEEE/RSJ International Conference on Intelligent Robots and System*, Vol. 1, pp. 835–840.
- Bailly, Y. and Amirat, Y. (2005). Modeling and control of a hybrid continuum active catheter for aortic aneurysm treatment. *IEEE International Conference on Robotics and Automation*, pp. 936–941.
- Bishop, R. L. (1975). There is more than one way to frame a curve. *The American Mathematical Monthly*, **82**: 246–251.
- Bostelman, R. V., Albus, J. S. and Graham, R. E. (1997). Robo-crane and EMMA applied to waste storage tank remediation. *American Nuclear Society Seventh Topical Meeting on Robotics and Remote Systems*, Vol. 2, pp. 708–713.
- Braganza, D., McIntyre, M., Dawson, D. and Walker, I. (2006). Whole arm grasping control for redundant robot manipulators. *American Control Conference*, pp. 3194–3199.
- Buckingham, R. (2002). Snake arm robots. *Industrial Robot: An International Journal*, **29**(3): 242–245.
- Burdette, E. C., Rucker, D. C., Prakash, P., Diederich, C. J., Croom, J. M., Clarke, C., Stolka, P., Juang, T., Bector, E. M., and Webster, R. J., III (2010). The ACUSITT ultrasonic ablator: the first steerable needle with an integrated interventional tool. *Proceedings of SPIE Medical Imaging*, 7629.
- Camarillo, D. B., Carlson, C. R. and Salisbury, J. K. (2009a). Configuration tracking for continuum manipulators with coupled tendon drive. *IEEE Transactions on Robotics*, **25**(4): 798–808.
- Camarillo, D. B., Carlson, C. R. and Salisbury, J. K. (2009b). Task-space control of continuum manipulators with coupled tendon drive. *11th International Symposium on Experimental Robotics 2008 (Springer Tracts in Advanced Robotics, Vol. 54)*. Berlin, Springer, pp. 271–280.
- Camarillo, D. B., Milne, C. F., Carlson, C. R., Zinn, M. R. and Salisbury, J. K. (2008). Mechanics modeling of tendon-driven continuum manipulators. *IEEE Transactions on Robotics*, **24**(6): 1262–1273.
- Chen, G., Pham, M. T., Herve, T. R. and Prelle, C. (2005). Design and modeling of a micro-robotic manipulator for colonoscopy. *5th International Workshop on Research and Education in Mechatronics*, Annecy, France, pp. 109–114.
- Chen, G., Pham, M. T. and Redarce, T. (2006). Development and kinematic analysis of a silicone-rubber bending tip for colonoscopy. *IEEE/RSJ International Conference on Intelligent Robots and Systems*, pp. 168–173.
- Chen, G., Thomann, G., Pham, M., Betemps, M. and Redarce, T. (2004). Modeling and control of a colonoscopic tip under disturbance of the insertion of colonoscope. *IEEE/RSJ International Conference on Intelligent Robots and Systems*, Vol. 4, pp. 3315–3320.
- Chirikjian, G. S. and Burdick, J. W. (1995). Kinematically optimal hyper-redundant manipulator configurations. *IEEE Transactions on Robotics and Automation*, **11**(6): 794–806.
- Chirikjian, G. S. (1995). Hyper-redundant manipulator dynamics: a continuum approximation. *Advanced Robotics*, **9**(3): 217–243.
- Chirikjian, G. S. and Burdick, J. W. (1994). A modal approach to hyper-redundant manipulator kinematics. *IEEE Transactions on Robotics and Automation*, **10**(3): 343–353.
- Chitrakaran, V. K., Behal, A., Dawson, D. M. and Walker, I. D. (2007). Setpoint regulation of continuum robots using a fixed camera. *Robotica*, **25**(5): 581–586.
- Choset, H. and Henning, W. (1999). A follow-the-leader approach to serpentine robot motion planning. *ASCE Journal of Aerospace Engineering*, **12**(2): 65–73.
- Cieślak, R. and Morecki, A. (1999). Elephant trunk type elastic manipulator—a tool for bulk and liquid materials transportation. *Robotica*, **17**(1): 11–16.
- Croom, J. M., Rucker, D. C., Romano, J. M., and Webster, R. J., III (2010). Visual sensing of continuum robot shape using self-organizing maps. *IEEE International Conference on Robotics and Automation*, pp. 4591–4596.
- Csencsits, M., Jones, B. A., McMahan, W., Iyengar, V. and Walker, I. D. (2005). User interfaces for continuum robot arms. *IEEE/RSJ International Conference on Intelligent Robots and Systems*, pp. 3123–3130.
- Dario, P., Carrozza, M. C., Marcacci, M., D’Attanasio, S., Magnani, B., Tonet, O. and Megali, G. (2000). A novel mechatronic tool for computer-assisted arthroscopy. *IEEE Transactions on Information Technology in Biomedicine*, **4**(1): 15–29.
- Degani, A., Choset, H., Wolf, A., Ota, T., and Zenati, M. A. (2006). Percutaneous intrapericardial interventions using a highly articulated robotic probe. *IEEE/RAS-EMBS International Conference on Biomedical Robotics and Biomechatronics*, pp. 7–12.
- Dupont, P. E., Lock, J. and Butler, E. (2009). Torsional kinematic model for concentric tube robots. *IEEE International Conference on Robotics and Automation*, pp. 3851–3858.
- Dupont, P. E., Lock, J., Itkowitz, B. and Butler, E. (2010). Design and control of concentric tube robots. *IEEE Transactions on Robotics*, in press.
- Ebeert-Uphoff, I. and Chirikjian, G. (1996). Inverse kinematics of discretely actuated hyper-redundant manipulators using workspace densities. *IEEE International Conference on Robotics and Automation*, pp. 139–145.
- Gravagne, I. A. (2002). *Design, Analysis and Experimentation: the Fundamentals of Continuum Robotic Manipulators*. PhD thesis, Clemson University.

- Gravagne, I. A., Rahn, C. and Walker, I. D. (2003). Large-deflection dynamics and control for planar continuum robots. *IEEE/ASME Transactions on Mechatronics*, **8**(2): 299–307.
- Gravagne, I. A. and Walker, I. D. (2002). Manipulability, force, and compliance analysis for planar continuum robots. *IEEE Transactions on Robotics and Automation*, **18**(3): 263–273.
- Hannan, M. W. and Walker, I. D. (2003). Kinematics and the implementation of an elephant's trunk manipulator and other continuum style robots. *Journal of Robotic Systems*, **20**(2): 45–63.
- Harada, K., Bo, Z., Enosawa, S., Chiba, T. and Fujie, M. (2007). Bending laser manipulator for intrauterine surgery and viscoelastic model of fetal rat tissue. *IEEE International Conference on Robotics and Automation*, pp. 611–616.
- Hirose, S. (1993). *Biologically Inspired Robots, Snake-Like Locomotors and Manipulators*. Oxford, Oxford University Press.
- Hirose, S. and Ma, S. (1991). Coupled tendon-driven multijoint manipulator. *IEEE International Conference on Robotics and Automation*, Vol. 2, pp. 1268–1275.
- Hirose, S. and Yamada, H. (2009). Snake-like robots. *IEEE Robotics and Automation Magazine*, **16**(1): 88–98.
- Ikuta, K., Tsukamoto, M. and Hirose, S. (1988). Shape memory alloy servo actuator system with electric resistance feedback and application for active endoscope. *IEEE International Conference on Robotics and Automation*, pp. 427–430.
- Immega, G. (1994). Tentacle-like manipulators with adjustable tension lines. U.S. Patent 5,317,952.
- Immega, G. and Antonelli, K. (1995). The KSI tentacle manipulator. *IEEE International Conference on Robotics and Automation*, Vol. 3, pp. 3149–3154.
- Immega, G., Antonelli, K. and Ko, J. (1995). Teleoperation of the KSI tentacle manipulator for hot cell decontamination. *Proceedings of the IEEE International Conference on Intelligent Systems for the 21st Century*, Vancouver, Canada, Vol. 3, pp. 2133–2136.
- Ivanescu, M., Florescu, M. C., Popescu, N. and Popescu, D. (2007). Coil function control problem for a hyperredundant robot. *IEEE/ASME International Conference on Advanced Intelligent Mechatronics*, pp. 1–6.
- Ivanescu, M. and Stoian, V. (1995). A variable structure controller for a tentacle manipulator. *Proceedings of the IEEE International Conference on Robotics and Automation*, Nagoya, Japan, Vol. 3, pp. 3155–3160.
- Jones, B. A., Gray, R. and Turlapati, K. (2009). Real-time statics for continuum robots. *IEEE/RSJ International Conference on Intelligent Robots and Systems*, pp. 2659–2664.
- Jones, B. A., McMahan, W. and Walker, I. D. (2006). Practical kinematics for real-time implementation of continuum robots. *IEEE International Conference on Robotics and Automation*, pp. 1840–1847.
- Jones, B. A. and Walker, I. D. (2006a). Kinematics for multisection continuum robots. *IEEE Transactions on Robotics*, **22**(1): 43–55.
- Jones, B. A. and Walker, I. D. (2006b). Practical kinematics for real-time implementation of continuum robots. *IEEE Transactions on Robotics*, **22**(6): 1087–1099.
- Jones, B. A. and Walker, I. D. (2007). Limiting-case analysis of continuum trunk kinematics. *IEEE International Conference on Robotics and Automation*, pp. 1363–1368.
- Kallem, V. and Cowan, N. J. (2009). Image guidance of flexible tip-steerable needles. *IEEE Transactions on Robotics*, **25**: 191–196.
- Kapoor, A. (2007). *Motion Constrained Control of Robots for Dexterous Surgical Tasks*. PhD thesis, Department of Computer Science, The Johns Hopkins University.
- Kim, J. S. and Chirikjian, G. S. (2006). Conformational analysis of stiff chiral polymers with end-constraints. *Molecular Simulation*, **32**(14): 1139–1154.
- Lane, D. M., Davies, J. B. C., Robinson, G., O'Brien, D. J., Sneddon, J., Seaton, E. and Elfstrom, A. (1999). The Amadeus dextrous subsea hand: design, modeling, and sensor processing. *IEEE Journal of Oceanic Engineering*, **24**(1): 96–111.
- Lang, H., Linn, J. and Arnold, M. (2009). Multibody dynamics simulation of geometrically exact Cosserat rods. *Multibody Dynamics 2009, ECCOMAS Thematic Conference*, Warsaw, Poland.
- Larson, O. and Davidson, C. (1985). Flexible arm, particularly a robot arm. U.S. Patent 4,494,417.
- Li, C. and Rahn, C. D. (2002). Design of continuous backbone, cable-driven robots. *ASME Journal of Mechanical Design*, **124**(2): 265–271.
- Lyons, L., Webster, R. J., III and Alterovitz, R. (2009). Motion planning for active cannulas. *IEEE/RSJ International Conference on Intelligent Robots and Systems*, pp. 801–806.
- Mochiyama, H., Shimemura E., and Kobayashi, H. (1999). Shape control of manipulators with hyper degrees of freedom. *The International Journal of Robotics Research*, **18**(6): 584–600.
- Moran, M. E. (2007). Evolution of robotic arms. *Journal of Robotic Surgery*, **1**(2): 103–111.
- Morecki, A., Jaworek, K., Pogorzelski, W., Zielinska, T. and Fraczek, J. (1987). Robotic System - Elephant Trunk Type Elastic Manipulator combined with a Quadruped Walking Machine. *Proceedings of the Second International Conference on Robotics and Factories of the Future*, pp. 649–656.
- Murray, R. M., Li, Z. and Sastry, S. S. (1994). *A Mathematical Introduction to Robotic Manipulation*. Boca Raton, FL, CRC Press.
- Nakamura, Y., Matsui, A., Saito, T. and Yoshimoto, K. (1995). Shape-memory-alloy active forceps for laparoscopic surgery. *IEEE International Conference on Robotics and Automation*, pp. 2320–2327.
- Neppalli, S., Csencsits, M. A., Jones, B. A. and Walker, I. D. (2009). Closed-form inverse kinematics for continuum manipulators. *Advanced Robotics*, **23**: 2077–2091.
- Neppalli, S. and Jones, B. A. (2007). Design, construction, and analysis of a continuum robot. *IEEE/RSJ International Conference on Intelligent Robots and Systems*, pp. 1503–1507.
- Nocks, L. (2007). *The Robot: The Life Story of a Technology (Greenwood Technographies)*. Westport, CT, Greenwood Press.
- OC Robotics, (2008). Snake-arm robots access the inaccessible. *Nuclear Technology International*, **1**: 92–94.

- Ohno, H. and Hirose, S. (2000). Study on slime robot (proposal of slime robot and design of slim slime robot). *Proceedings of the IEEE/RSJ International Conference on Intelligent Robots and Systems*, Vol. 3, pp. 2218–2223.
- Ohno, H. and Hirose, S. (2001). Design of slim slime robot and its gait of locomotion. *Proceedings of the IEEE/RSJ International Conference on Intelligent Robots and Systems*, Vol. 2, pp. 707–715.
- Ohta, R. (2001). Results of R & D on catheter-type micromachine. *International Symposium on Micromechatronics and Human Science*, pp. 5–12.
- Osuka, K. and Kitajima, H. (2003). Development of mobile inspection robot for rescue activities: MOIRA. *IEEE/RSJ International Conference on Intelligent Robots and Systems*, pp. 3373–3377.
- Paljug, E., Ohm, T. and Hayati, S. (1995). The JPLs serpentine robot: a 12-DOF system for inspection. *IEEE International Conference on Robotics and Automation*, Vol. 3, pp. 3143–3148.
- Park, J. and Chung, W.-K. (2005). Geometric integration on Euclidean group with application to articulated multibody systems. *IEEE Transactions on Robotics*, **21**(5): 850–863.
- Peirs, J., Reynaerts, D., Brussel, H. V., Gerssem, G. D. and Tang, H. T. (2003). Design of an advanced tool guiding system for robotic surgery. *IEEE International Conference on Robotics and Automation*, pp. 2651–2656.
- Phee, S. J., Ng, W. S., Chen, I. M., Seow-Choen, F. and Davies, B. L. (1997). Locomotion and steering aspects in automation of colonoscopy part one: a literature review. *IEEE Engineering in Medicine and Biology Magazine*, **16**(6): 85–96.
- Reed, K., Kallem, V., Alterovitz, R., Goldberg, K., Okamura, A. M. and Cowan, N. J. (2008). Integrated planning and image-guided control for planar needle steering. *IEEE RAS/EMBS International Conference on Biomedical Robotics and Biomechatronics*, Scottsdale, AZ, pp. 819–824.
- Robinson, G. and Davies, J. B. C. (1999). Continuum robots—a state of the art. *IEEE International Conference on Robotics and Automation*, pp. 2849–2854.
- Rosheim, M. E. (1994). *Robot Evolution: The Development of Anthrobotics*. New York, NY, John Wiley & Sons.
- Rucker, D. C., Croom, J. M. and Webster, R. J., III (2009). Aiming surgical lasers with an active cannula. *ASME Journal of Medical Devices*, **3**(2): 027506.
- Rucker, D. C., Jones, B. A. and Webster, R. J., III (2010a). A geometrically exact model for externally loaded concentric tube continuum robots. *IEEE Transactions on Robotics*, accepted.
- Rucker, D. C. and Webster, R. J., III (2008). Mechanics-based modeling of bending and torsion in active cannulas. *IEEE RAS/EMBS International Conference on Biomedical Robotics and Biomechatronics*, pp. 704–709.
- Rucker, D. C. and Webster, R. J., III (2009a). Mechanics of bending, torsion, and variable precurvature in multi-tube active cannulas. *IEEE International Conference on Robotics and Automation* pp. 2533–2537.
- Rucker, D. C. and Webster, R. J., III (2009b). Parsimonious evaluation of concentric-tube continuum robot equilibrium conformation. *IEEE Transactions on Biomedical Engineering*, **56**(9): 2308–2311.
- Rucker, D. C., Webster, R. J., III, Chirikjian, G. S. and Cowan, N. J. (2010b). Equilibrium conformations of concentric-tube continuum robots. *International Journal of Robotics Research*, in press.
- Sears, P. and Dupont, P. E. (2006). A steerable needle technology using curved concentric tubes. In *IEEE/RSJ International Conference on Intelligent Robots and Systems*, Beijing, China, pp. 2850–2856.
- Sears, P. and Dupont, P. E. (2007). Inverse kinematics of concentric tube steerable needles. *IEEE International Conference on Robotics and Automation*, pp. 1887–1892.
- Simaan, N. (2005). Snake-like units using flexible backbones and actuation redundancy for enhanced minaturization. *IEEE International Conference on Robotics and Automation*, pp. 3023–3028.
- Simaan, N., Taylor, R. and Flint, P. (2004). A dexterous system for laryngeal surgery. *IEEE International Conference on Robotics and Automation*, pp. 351–357.
- Simaan, N., Xu, K., Wei, W., Kapoor, A., Kazanzides, P., Taylor, R. and Flint, P. (2009). Design and integration of a telerobotic system for minimally invasive surgery of the throat. *The International Journal of Robotics Research*, **28**(9): 1134–1153.
- Spillmann, J. and Teschner, M. (2007). Corde: Cosserat rod elements for the dynamic simulation of one-dimensional elastic objects. *SCA '07: Proceedings of the 2007 ACM SIGGRAPH/Eurographics Symposium on Computer Animation*, pp. 63–72.
- Suthakorn, J. and Chirikjian, G. S. (2001). A new inverse kinematics algorithm for binary manipulators with many actuators. *Advanced Robotics*, **15**(2): 225–244.
- Suzumori, K., Iikura, S. and Tanaka, H. (1992). Applying a flexible microactuator to robotic mechanisms. *IEEE Control Systems Magazine*, **12**(1): 21–27.
- Suzumori, K., Wakimoto, S. and Takata, M. (2003). A miniature inspection robot negotiating pipes of widely varying diameter. *IEEE International Conference on Robotics and Automation*, pp. 2735–2740.
- Takahashi, M., Hayashi, I., Iwatsuki, N., Suzumori, K. and Ohki, N. (1994). The development of an in-pipe microrobot applying the motion of an earthworm. *International Symposium on Micro Machine and Human Science*, pp. 35–40.
- Tatlicioglu, E., Walker, I. D. and Dawson, D. M. (2007). New dynamic models for planar extensible continuum robot manipulators. *Proceedings of the 2007 IEEE/RSJ International Conference on Intelligent Robots and Systems*, pp. 1485–1490.
- Thring, M. (1983). *Robots and Telechairs; Manipulators with Memory; Remote Manipulators; Machine Limbs for the Handicapped* Chichester, Ellis Horwood.
- Transeth, A. A., Pettersen, K. Y. and Liljeback, P. (2009). A survey on snake robot modeling and locomotion. *Robotica*, **27**: 999–1015.
- Trivedi, D., Lotfi, A. and Rahn, C. D. (2008a). Geometrically exact models for soft robotic manipulators. *IEEE Transactions on Robotics*, **24**(4): 773–780.
- Trivedi, D., Rahn, C. D., Kierb, W. M. and Walker, I. D. (2008b). Soft robotics: biological inspiration, state of the art, and future research. *Applied Bionics and Biomechanics*, **5**(3): 99–117.

- Tsukagoshi, H., Kitagawa, A. and Segawa, M. (2001). Active hose: an artificial elephant's nose with maneuverability for rescue operation. *Proceedings of the IEEE International Conference on Robotics and Automation*, Seoul, Korea, Vol. 3, pp. 2454–2459.
- Wakahara, Y., Asano, K. and Tsuchihashi, T. (1984). A computer aided manipulation system for a multijoint inspection robot. *Transactions of the American Nuclear Society*, **47**: 455–456.
- Webster, R. J., III (2007). *Design and Mechanics of Continuum Robots for Surgery*. PhD Thesis, Mechanical engineering, The Johns Hopkins University, Baltimore, MD.
- Webster, R. J., III, Kim, J. S., Cowan, N. J., Chirikjian, G. S. and Okamura, A. M. (2006a). Nonholonomic modeling of needle steering. *The International Journal of Robotics Research*, **25**(5/6): 509–526.
- Webster, R. J., III, Memisevic, J. and Okamura, A. M. (2005). Design considerations for robotic needle steering. *IEEE International Conference on Robotics and Automation*, pp. 3599–3605.
- Webster, R. J., III, Okamura, A. M. and Cowan, N. J. (2006b). Toward active cannulas: miniature snake-like surgical robots. *IEEE/RSJ International Conference on Intelligent Robots and Systems*, pp. 2857–2863.
- Webster, R. J., III, Romano, J. M. and Cowan, N. J. (2009). Mechanics of precurved-tube continuum robots. *IEEE Transactions on Robotics*, **25**(1): 67–78.
- Webster, R. J., III, Swenson, J. P., Romano, J. M. and Cowan, N. J. (2008). Closed-form differential kinematics for concentric-tube continuum robots with application to visual servoing. *11th International Symposium on Experimental Robotics 2008 (Springer Tracts in Advanced Robotics, Vol. 54)*. Berlin, Springer, pp. 485–494.
- Wilson, J. F., Li, D., Chen, Z. and R. T. George, J. (1993). Flexible robot manipulators and grippers: relatives of elephant trunks and squid tentacles. *Robots and Biological Systems: Towards a New Bionics?*, Dario, P., Sandini, G. and Aebischer, P. (eds) (*NATO ASI Series*, Vol. 102). Berlin, Springer, pp. 475–494.
- Wolf, A., Brown, H. B., Casciola, R., A. Costa, M. S., Shamas, E. and Choset, H. (2003). A mobile hyper redundant mechanism for search and rescue tasks. *IEEE/RSJ International Conference on Intelligent Robots and Systems*, pp. 2889–2895.
- Wright, C., Johnson, A., Peck, A., McCord, Z., Naaktgeboren, A., Gianfortoni, P., Gonzalez-Rivero, M., Hatton, R. and Choset, H. (2007). Design of a modular snake robot. *IEEE/RSJ International Conference on Intelligent Robots and Systems*, pp. 2609–2614.
- Xu, K. and Simaan, N. (2006). Actuation compensation for flexible surgical snake-like robots with redundant remote actuation. *IEEE International Conference on Robotics and Automation*, pp. 4148–4154.
- Xu, K. and Simaan, N. (2008). An investigation of the intrinsic force sensing capabilities of continuum robots. *IEEE Transactions on Robotics*, **24**(3): 576–587.